

A Review on the Conventional Capacitors, Supercapacitors, and Emerging Hybrid Ion Capacitors: Past, Present, and Future

Jiale Sun, Bingcheng Luo,* and Huanxin Li*

Electrochemical energy storage (EES) devices with high-power density such as capacitors, supercapacitors, and hybrid ion capacitors arouse intensive research passion. Recently, there are many review articles reporting the materials and structural design of the electrode and electrolyte for supercapacitors and hybrid capacitors (HCs), though these reviews always focus on individual supercapacitors or single HCs. Herein, the conventional capacitor, supercapacitor, and hybrid ion capacitor are incorporated, as the detailed description of conventional capacitors is very fundamental and necessary for the better understanding and development of supercapacitors and hybrid ion capacitors, which are often ignored. Therefore, herein, the fundamentals and recent advances of conventional capacitors, supercapacitors, and emerging hybrid ion capacitors are comprehensively and systematically summarized in terms of history, mechanisms, electrode materials, existing challenges, and perspectives. At the same time, it is believed that a comprehensive and fundamental understanding for capacitor-related EES devices is provided in the review and has a great guiding role for future development.

1. Introduction

Threatened by the increasing scarcity of fossil fuels and deteriorating environmental pollution, people have begun to work on

exploiting clean and reproducible natural energy, including solar, wind, tidal energy, and so on.^[1] Nevertheless, this kind of renewable energies are closely relevant to the natural conditions and cannot be afforded continuously and steadily. Therefore, novel electrochemical energy-storage (EES) devices are required to collect and store these renewable energies. Batteries and supercapacitors are some of the most protruding and promising EES devices owing to the superior energy density and power density, respectively.^[2,3] Although the batteries have a great range of applications in electric vehicles and electronic products, the inferior power density and poor cycling stability restrict their commercial applications to some extent. To compromise the drawbacks of batteries, supercapacitors became the research hotspot derived from its remarkable power

density, rapid charge/discharge rate, and excellent durability.^[4,5]


When it comes to supercapacitors, we must first have a sufficient understanding of conventional capacitors, because the essence of supercapacitors is inseparable from conventional capacitors. The conventional capacitors, as a passive electronic component, have been extensively applied to the electronic circuits and pulse power applications for their ultrahigh-power density, extremely rapid charge/discharge rates, and superior service lifetime.^[6,7] Although the capacitors and supercapacitors behave at the protruding power density, their inferior energy density compared to batteries makes them hard to satisfy the requirements for mobile energy-storage devices. Therefore, the appearance of emerging capacitors containing metal ion hybrid capacitors (HCs) and dual-ion capacitors (DICs) is expected to enlarge energy density without weakening power density.^[8]

For the conventional capacitors, supercapacitors, and emerging capacitors, the electrode materials or dielectric materials are one of the most paramount components for affecting their electrochemical performance. Hence, the breakthrough in electrode and dielectric materials promoted the development of EES devices.^[9] For example, the initial research of conventional capacitors was only focused on ceramics, glass, and polymer dielectrics. With the increasing demand and the respective drawbacks of a single material, ceramics and polymer-based composite dielectrics appeared in the people's vision.^[10–13] Furthermore, a large number of lead-free dielectrics continually

J. Sun, H. Li
State Key Laboratory for Chemo/Biosensing and Chemometrics
College of Chemistry and Chemical Engineering
Hunan University
Changsha, Hunan 410082, China
E-mail: lihuanxin@hnu.edu.cn, hl583@cam.ac.uk

B. Luo
College of Science
China Agricultural University
Beijing 100083, P. R. China
E-mail: luobc21@cau.edu.cn

H. Li
Department of Engineering
University of Cambridge
9 JJ Thomson Avenue, Cambridge CB3 0FA, UK

 The ORCID identification number(s) for the author(s) of this article can be found under <https://doi.org/10.1002/aesr.202100191>.

© 2022 The Authors. Advanced Energy and Sustainability Research published by Wiley-VCH GmbH. This is an open access article under the terms of the Creative Commons Attribution License, which permits use, distribution and reproduction in any medium, provided the original work is properly cited.

DOI: 10.1002/aesr.202100191

emerged when considering the toxicity of lead.^[14–17] Up to now, the dielectrics with high permittivity and breakdown strength are still in intense research. Regarding the supercapacitors, the carbon materials with high specific surface area were bearing the brunt. Then, the appearance of conduct polymers and transition metal oxides was employed to enlarge specific capacitance and specific energy. Presently, the concept about “battery type” electrode materials was proposed based on the depth research of charge-storage mechanism and electrochemical behavior.^[18] Meanwhile, some emerging electrode materials including Mxene, transition-metal dichalcogenides (TMDs), and metal nitride/phosphide are also being extensively studied.^[19,20] Certainly, the improvement of electrode materials is still in progress, including element doping, defect construction, and composites. Throughout the history of the development of EES equipment, it is inseparable from the development of electrode materials. Although the other components are equally important to the performance of EES devices, including electrolyte, separator, and current collector, this minireview will mainly introduce the development of electrode materials due to space limitations.

In recent years, many reviews about single conventional capacitors, single supercapacitors, and single metal ion HCs have been widely reported. However, the comprehensive review for conventional capacitors, supercapacitors, and emerging hybrid ion capacitors has received little concern. Hence, the minireview aims to give scholars an integrated understanding for all types of capacitors. This minireview concisely introduces the development history and storage mechanism about conventional capacitors, supercapacitors, emerging hybrid ion capacitors, and the development of the corresponding electrode materials, respectively (Figure 1). Finally, we summarize and look forward

to the further development of conventional capacitors, supercapacitors, and emerging hybrid ion capacitors. Hopefully, from the history, we can see the future.

2. Conventional Capacitors

The conventional capacitors, as a passive electronic component, are composed of two adjacent conductors and an insulating medium between them. In 1745, the invention of the Leyden jar opened the door of capacitor technology.^[21] Thereafter, a series of representative capacitors came out one after another. In 1876, the paper capacitors were constructed by placing a waxed paper among metal foils and firmly rolling it into the circular column.^[22] In 1896, the first electrolytic capacitor was patented by using a less impurity etching aluminum leaf with alumina as dielectric.^[23] Some prominent capacitors have also appeared in succession including mica dielectric capacitor (1909), polyethylene terephthalate-based capacitor (1941), and plastic dielectric capacitor (1959).^[24] At first, capacitors are mainly used in electrical and electronic commodities, but currently they are utilized for various domain involving vehicles, aircraft, aerospace, medical, and power grids based on their ultrahigh-power density, extremely rapid charge–discharge rates, and superior service life.^[25]

Dielectric capacitors and electrolytic capacitors are two common conventional capacitors. The medium of a dielectric capacitor is a dielectric material, which relies on the polarization of the dipole around the electrode and dielectric interface to store charge (Figure 2a). The medium of an electrolytic capacitor is a solid or liquid ionic conductor, usually called an electrolyte. As delineated in Figure 2b, it accumulates cations at the interface around the negative electrode and electrolyte, meanwhile the same amount of anions at the interface around the positive electrode and electrolyte to achieve the purpose of storing charge.^[26] In contrast, owing to the wide variety of batteries, we took a lithium-ion battery as an example to elaborate its charge-storage mechanism. As illustrated in Figure 2c, the lithium-ion battery store energy through a “rocking-chair” mechanism that the lithium ions is repeatedly deintercalated/intercalated from the lithium-containing transition metal oxide cathode and intercalate/deintercalated into the interlayer of the graphite anode through the electrolyte during the charge/discharge reaction.^[27] The competence of charge-storage for a capacitor is measured by the value of capacitance. As shown in Equation (1), the capacitance of a capacitor is proportional to the area between the electrode and the dielectric (A), and inversely proportional to the distance between the two plates (d).

$$C = \epsilon_0 \epsilon_r A / d \quad (1)$$

Herein, ϵ_0 and ϵ_r are the vacuum and relative permittivity, respectively.

Since electrolytic capacitors have more movable free electrons than dielectric capacitors, electrolytic capacitors possess larger capacitance. Normally, the capacitance of an electrolytic capacitor is in the order of millifarad (mF), and the capacitance of a dielectric capacitor is in the order of microfarad (μ F).

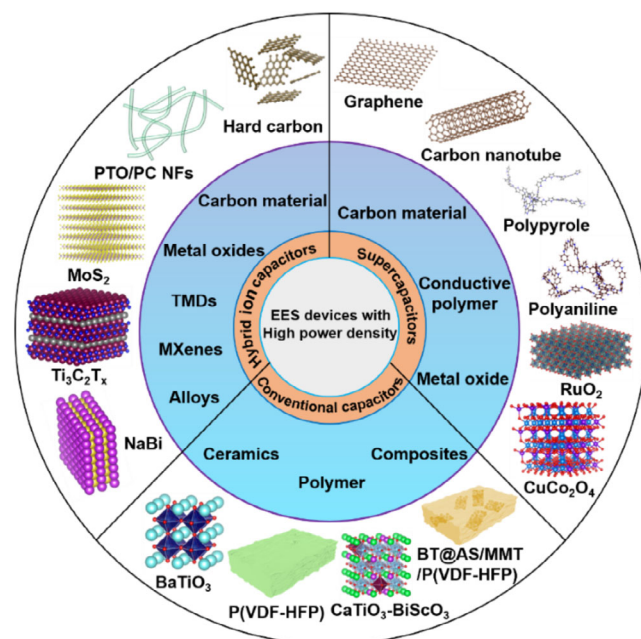


Figure 1. Schematic diagram of the available electrodes and dielectric for the conventional capacitors, supercapacitors, and emerging hybrid ion capacitors summarized from the recent literature.

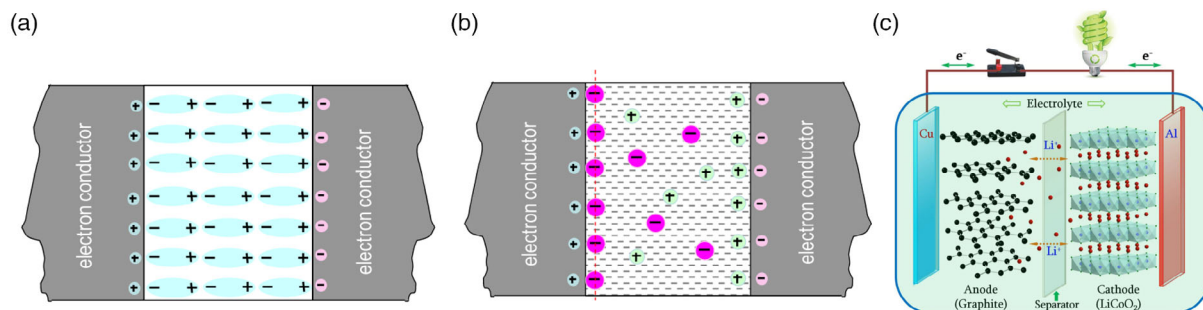


Figure 2. Schematic diagram of charge storage in conventional capacitors and lithium-ion battery. a) dielectric capacitor. b) electrolytic capacitor. Reproduced with permission.^[26] Copyright 2013, Elsevier BV. c) Lithium-ion battery. Reproduced with permission.^[27] Copyright 2016, Elsevier.

Normally, the energy density about capacitor (U_e) is acquired under Equation (2).

$$U_e = \epsilon_0 \epsilon_r E_b^2 / 2 \quad (2)$$

where E_b is the breakdown strength. Therefore, the development of advanced dielectric materials with the increased permittivity and higher breakdown strength is a crucial measure to raise the energy density of capacitors.

Recently, the different dielectric materials have motivated the development of advanced capacitors, such as polymers, ceramics, and their composites.^[6,28–32] Without exception, while these dielectric materials exert their advantages, they also have their

shortcomings. For example, the polymer dielectrics exhibited the superiorities of strong breakdown field, low dielectric wastage, convenient processability, and mechanical flexibility, but they suffered from the drawbacks of inferior permittivity and weak thermal stability. The polyvinylidene fluoride and its copolymers, biaxially oriented polypropylene (BOPP), polyethylene terephthalate, polycarbonate, and polyimide were the common polymer dielectrics for the capacitors.^[31,33,34] Through blending poly (vinylidene fluoride-hexafluoropropylene) (P(VDF-HFP)) with poly (methylmethacrylate) (PMMA), enhanced energy-storage performance can be obtained. As shown in **Figure 3**, the P(VDF-HFP)/PMMA mixed films of 42.6 vol% PMMA displayed a discharged energy density as

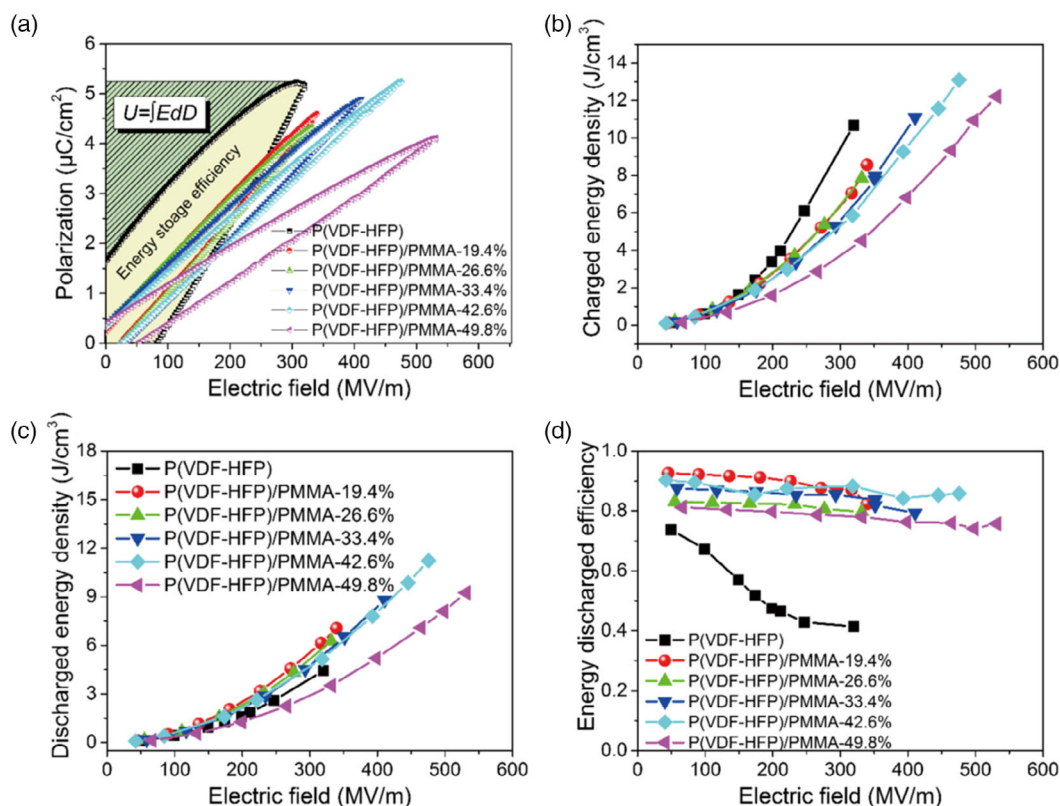


Figure 3. a) Maximum polarization, b) charging specific energy, c) discharging specific energy, d) energy efficiency about single P(VDF-HFP), and P(VDF-HFP)/PMMA mixed films at diverse compositions. Reproduced with permission.^[31] Copyright 2017, Elsevier BV.

11.2 J cm^{-3} and 85.8% efficiency under an electric field of 475 MV m^{-1} , which is ≈ 5 times higher than commercial BOPP capacitors.^[31]

The ceramics dielectrics possessed high permittivity and good thermal stability but suffered low breakdown strength.^[35,36] The lead-based ceramics as $(1-x)[\text{Pb}(\text{Mg}_{1/3}\text{Nb}_{2/3})\text{O}_3]-x[\text{PbTiO}_3]$ (PMN-PT), $(\text{Pb}_{1-x}\text{La}_x)(\text{Zr}_y\text{Ti}_{1-y})_{1-x/4}\text{O}_3$ (PLZT), and $\text{PbZr}_{1-x}\text{Ti}_x\text{O}_3$ (PZT), and lead-free ceramics as BaTiO_3 , AgNbO_3 , and NaNbO_3 have been widely studied for the capacitors.^[37] An emerging lead-free $(1-x)\text{CaTiO}_3-x\text{BiScO}_3$ linear dielectric ceramic with reinforced volume specific energy was reported.^[38] As shown in **Figure 4**, the $0.9\text{CaTiO}_3-0.1\text{BiScO}_3$ ceramic achieved an energy density of 1.55 J cm^{-3} and 90.4% energy efficiency under a breakdown field of 270 kV cm^{-1} as well as a power density with 1.79 MW cm^{-3} .

The manufacturing of multiphase coexistence in ferroelectric (FE) ceramics was reported as one available method to accomplish

stable and high energy-storage performances. Zhu et al. designed the NaNbO_3 -modified $0.95\text{Bi}_{0.5}\text{Na}_{0.5}\text{TiO}_3-0.05\text{SrZrO}_3$ ceramics $((1-x)\text{BNTSZ}-x\text{NN})$ to realize the co-occurrence of rhombohedral and tetragonal phases (**Figure 5a-d**).^[39] A record-high upper operating temperature was achieved for the change of dielectric permittivity about the $0.8\text{BNTSZ}-0.2\text{NN}$ ceramic with a value under $\pm 15\%$ in the temperature extent of -55 to 545°C . At 120°C , the $0.85\text{BNTSZ}-0.15\text{NN}$ ceramic performed a volume specific energy with 3.14 J cm^{-3} and an energy efficiency of 79% under 230 kV cm^{-1} (**Figure 5e-h**).

To overcome the respective shortcomings and improve the energy-storage capability of capacitors, the development of dielectric composite materials was a very attractive approach, such as ceramics-based, polymer-based composites.^[40,41] The integration of ceramics with high permittivity and polymers with strong breakdown fields was hopeful to achieve an improved energy density in the composites. For example, Liu et al.

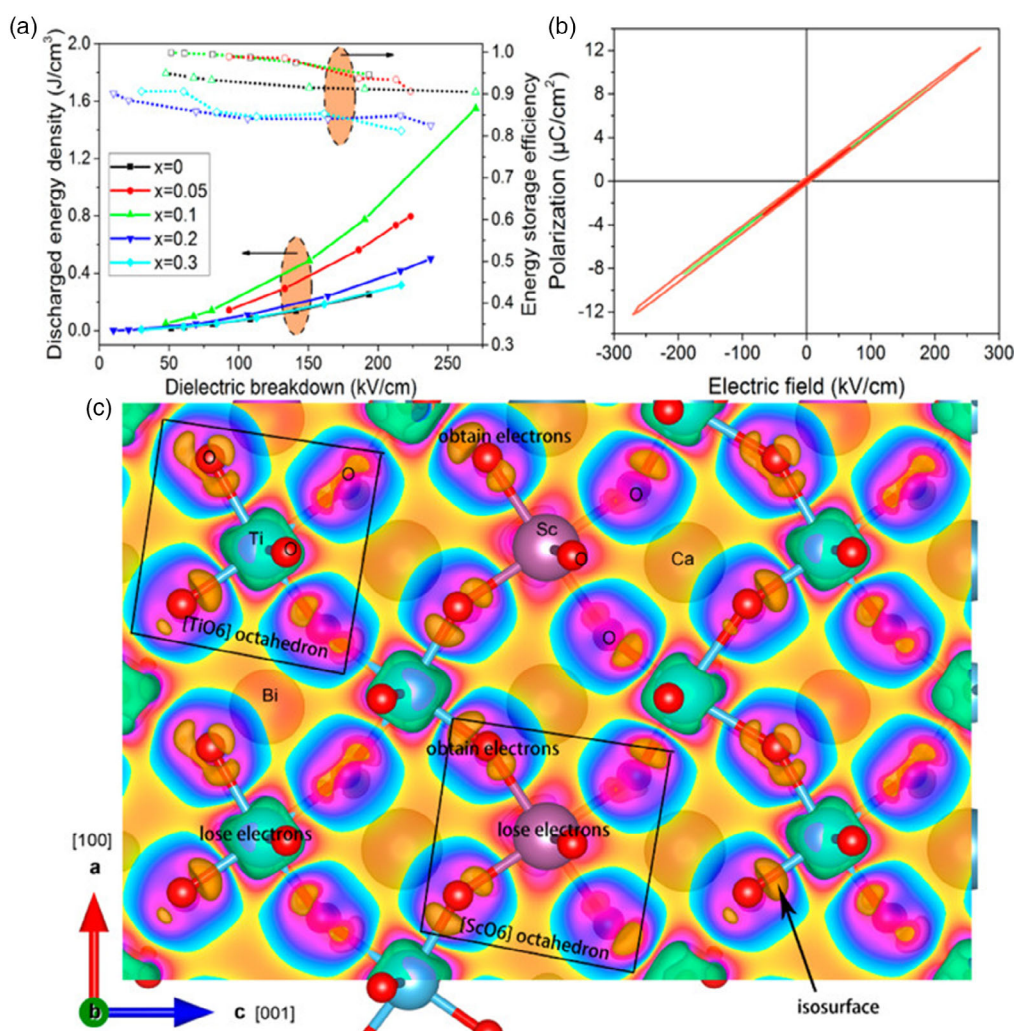


Figure 4. a) The relationship between the discharge energy density and energy efficiency for $\text{CaTiO}_3\text{-BiScO}_3$ ceramics and the breakdown field under various BiScO_3 constituent. b) P-E loops about $0.9\text{CaTiO}_3-0.1\text{BiScO}_3$ ceramics. c) Differential charge density about lead-free $\text{CaTiO}_3\text{-BiScO}_3$ dielectric crystal lattice. The charge density is drawn by the (010) from 0 (orange) to 1 (red) $\text{e} \text{ \AA}^{-3}$, and the related density isosurfaces presented as the spherical shadow. Oxygen atoms attain electrons, while titanium and scandium atoms lost electrons. Reproduced with permission.^[38] Copyright 2017, American Chemical Society.

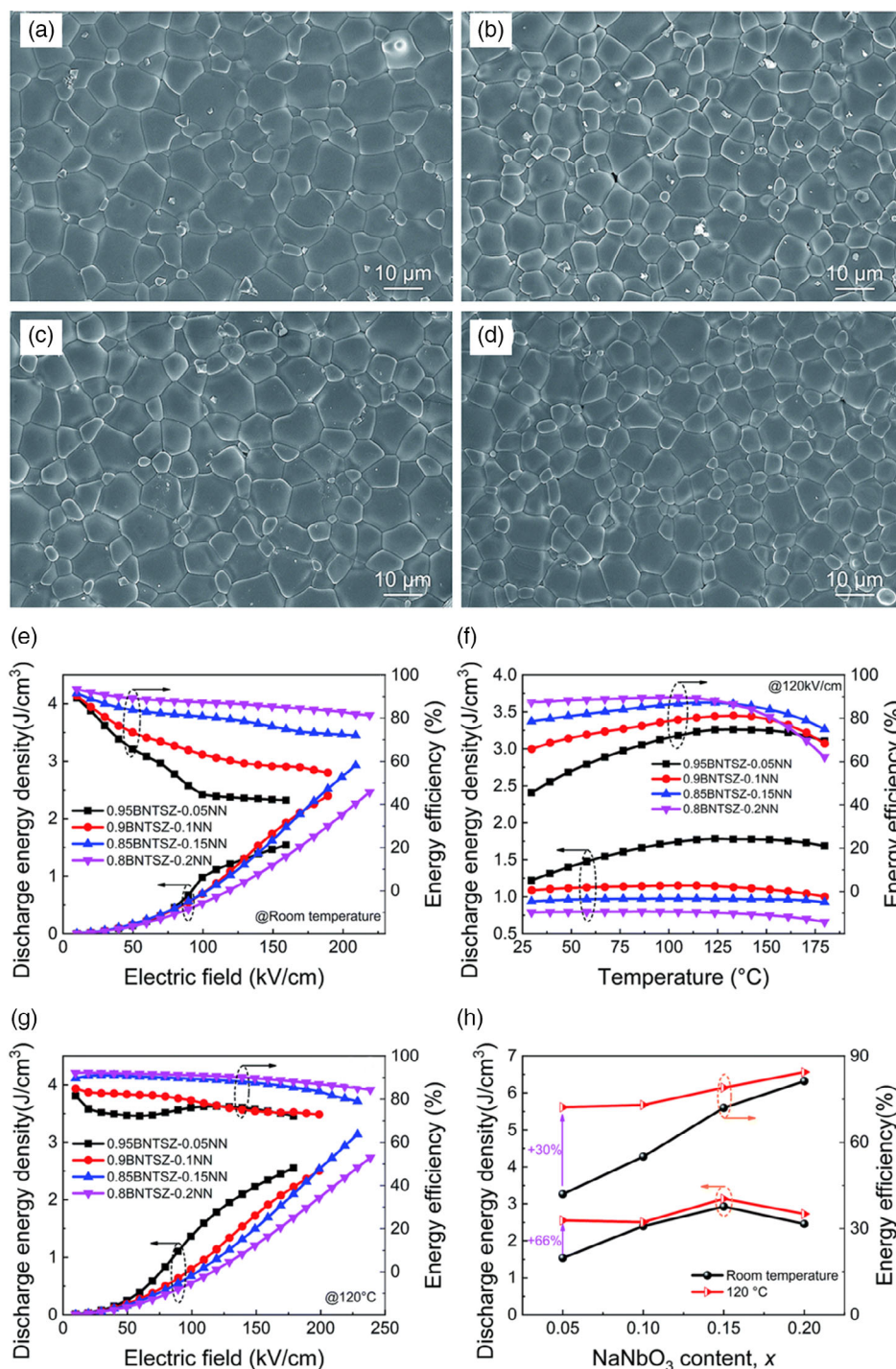


Figure 5. The scanning electron microscope (SEM) photograph for the NaNbO_3 -modified $0.95\text{Bi}_{0.5}\text{Na}_{0.5}\text{TiO}_3\text{-}0.05\text{SrZrO}_3$ ceramics ($(1-x)\text{BNTSZ-xNN}$) ceramics. a–d) $x = 0.05, 0.10, 0.15, 0.20$, respectively. e) The relationship between discharge volume specific energy and energy efficiency about the $(1-x)\text{BNTSZ-xNN}$ ceramics and the imposed electric field under normal temperature. f) The discharge volume specific energy and energy efficiency of various temperatures at $120\ \text{kV}\ \text{cm}^{-1}$. g) The discharge volume specific energy and energy efficiency with different imposed electric field under 120°C . h) The optimum discharge volume-specific energy and the related energy efficiency under different imposed electric fields under normal temperature and 120°C , respectively. All tests are performed at $1\ \text{Hz}$. Reproduced with permission.^[39] Copyright 2020, Royal Society of Chemistry.

comprehensively summarized the development of (semi)conductor/polymer composites from 0 to 3D (semi)conducting fillers.^[42] Zhang et al. illustrated the need and proposal of polymer-based

nanocomposite dielectrics and reviewed the critical material questions about two kinds of polymer nanodielectrics, polymer/conductive nanoparticle and polymer/ceramic nanoparticle

composites.^[43] High-performance dielectric composite capacitors were widely studied for the past decades. The composite materials emerged from other materials and became the core dielectrics of film capacitors due to their elasticity, low price, and tailored functional features. Fan et al. summarized the newest development about polymer-based film dielectrics and elaborated the methods in detail for improving the performance of polymer film from two aspects: nanocomposites and all-polymer dielectric films.^[44] Whereas, it has always been a long-term challenge to synchronously accomplish high volumetric-specific energy and efficiency when imposing the actually operated electric field. Luo et al. designed the superhierarchical nanocomposites based on FE perovskites, layered aluminosilicate nanosheets, and an organic polymer matrix, and achieved a high volumetric-specific energy of 20 J cm^{-3} with 84% efficiency

under 510 MV m^{-1} .^[45] When the electric field is less than 600 MV m^{-1} and the energy efficiency is greater than 80%, this value of volumetric specific energy is highest among all the most advanced dielectric polymer nanocomposites (Figure 6). In Palneedi's review, the comprehensive overview about linear dielectric, paraelectric (PE), FE, relaxor FE, and anti-FE ceramic was represented, and some appealing strategies containing physical, chemical, and microstructural alteration for dielectric ceramic films were discussed.^[46]

Currently, there has been a rapidly increasing demand for multilayer ceramics capacitors (MLCCs) in the smartphone, portable pseudocapacitors (PCs), and automotive industry, because the MLCCs can assign and regulate the amount of current flowing through circuits, eliminate noise, and avoid breakdown of electronic devices.^[47] The detailed structure diagram

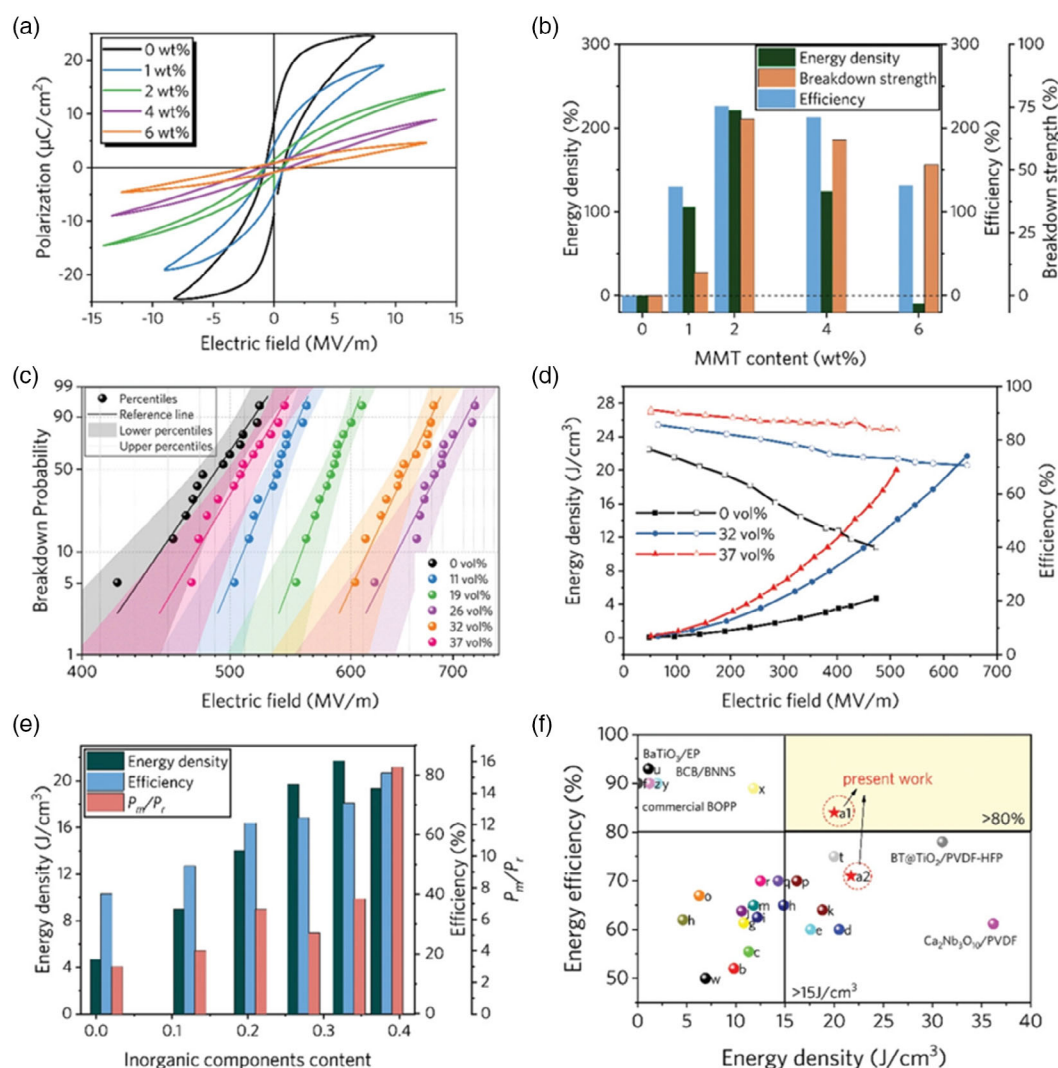


Figure 6. a) P–E loops about barium titanate (BT)/montmorillonite (MMT) ferroelectric (FE) ceramic composites under diverse MMT component. b) Improvement of discharge energy density, energy efficiency, and dielectric breakdown strength about BT/MMT FE ceramics. c) Weibull statistics about dielectric breakdown strength for BT@AS/MMT/P(VDF–HFP) nanocomposite films. d) Energy density and energy efficiency for BT@AS/MMT/P(VDF–HFP) nanocomposite films with different imposed electric fields. e) The energy-storage capability for BT@AS/MMT/P(VDF–HFP) nanocomposite films under diverse inorganic contents in the breakdown fields. f) The energy density and energy efficiency about dielectric polymer nanocomposites compared with earlier reported values. Reproduced with permission.^[45] Copyright 2021, Wiley-VCH Verlag.

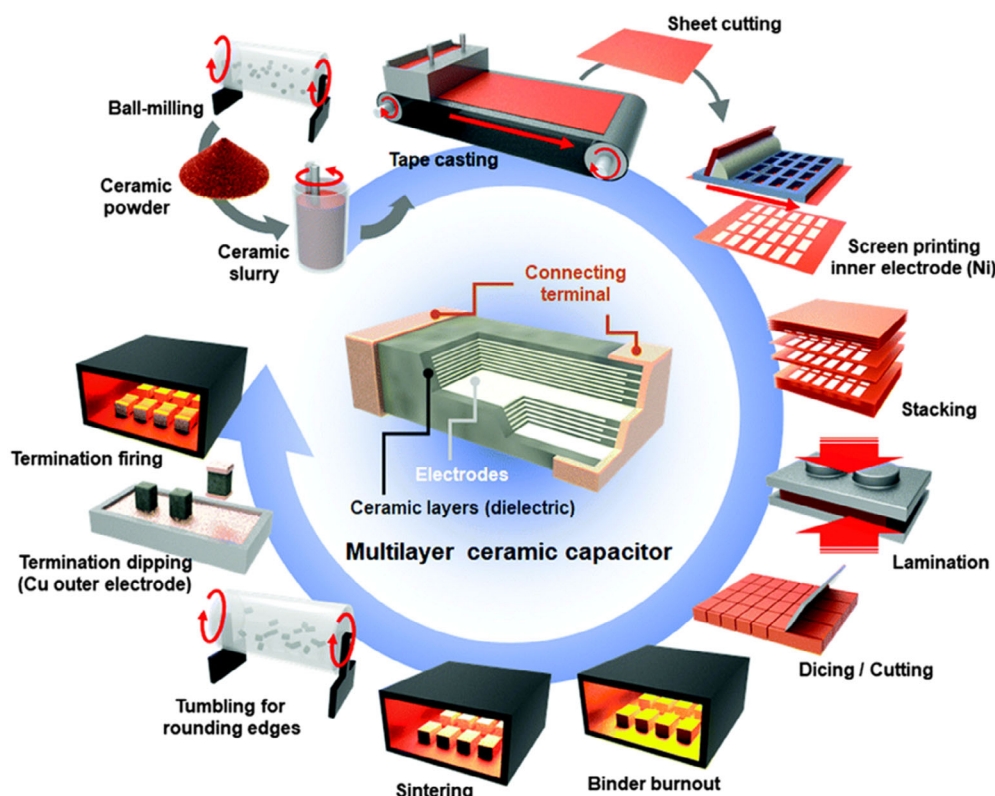


Figure 7. Schematics of multilayer ceramic capacitors (MLCCs) construction and its manufacturing process. Reproduced with permission.^[47] Copyright 2019, Royal Society of Chemistry.

and manufacturing process of MLCCs is displayed in **Figure 7**. This manufacturing technique is based on a powder material method suitable for large scale from laboratory study to commercial fabricating. A mass of works about MLCCs have been published, for example, Hong and coworker made a short description to MLCCs and dielectric materials and emphasized the key problems and latest progresses in the development of MLCCs with high volumetric efficiency and high capacitance from the perspective of engineering BaTiO₃-based dielectric layers.^[47] Feng et al. introduced the primary physical mechanisms about polarization, breakdown, and energy storage of multilayer structure dielectric, systematically summarized the theoretical simulation and experimental results, and described the synthesis approaches and design concepts about multilayer structure dielectrics.^[48] In addition, the film capacitors have aroused intensive research interests owing to their higher dielectric strength and volumetric specific energy than their bulk counterparts and this is because the dielectric strength increases as the decreasing of dielectrics thickness. Ceramic film capacitors with the smallest footprint are particularly suitable for microelectronic systems, mobile platforms, and miniaturized power devices. Compared with their bulk counterparts, ceramic films with dense, nonporous microstructures, and fewer defects and lattice defects can withstand strong electric fields, thereby showing greater volumetric specific energy. Several film preparation approaches about magnetron sputtering, pulsed laser deposition, sol-gel method, tape casting, chemical solution deposition,

screen printing, and atomic layer deposition have been used to the development about dielectric ceramic films in energy-storage capacitors.^[49]

Zhao et al. reported the multilayer ceramic capacitors (MLCCs) composed of 0.87BaTiO₃–0.13Bi(Zn_{2/3}(Nb_{0.85}Ta_{0.15})_{1/3})O₃@SiO₂ relaxor FE grain through multi-scale modification method from the atomic scale to grain-scale to device-scale designs to enlarge the breakdown field strength and reduce the current loss, which accomplishes excellent energy-storage capability including a great discharge volumetric specific energy of 18.24 J cm^{−3}, superhigh efficiency above 94.5%, prominent temperature stability, and cycle durability (**Figure 8**).^[50] More recently, Pan et al. illustrated the substantial enhancements of energy-storage properties in relaxor FE films with a super-PE design and achieved an energy density of 152 J cm^{−3} with improved efficiency (>90% at an electric field of 3.5 MV cm^{−1}) in super-PE samarium-doped bismuth ferrite–barium titanate films (**Figure 9**).^[51]

3. Supercapacitors

3.1. Origin and Development of Supercapacitors

Supercapacitors, also named as electrochemical capacitors, are a new type of EES device, different from conventional capacitors and batteries. In contrast with traditional capacitors, the area between the electrode and dielectric of the supercapacitors is very

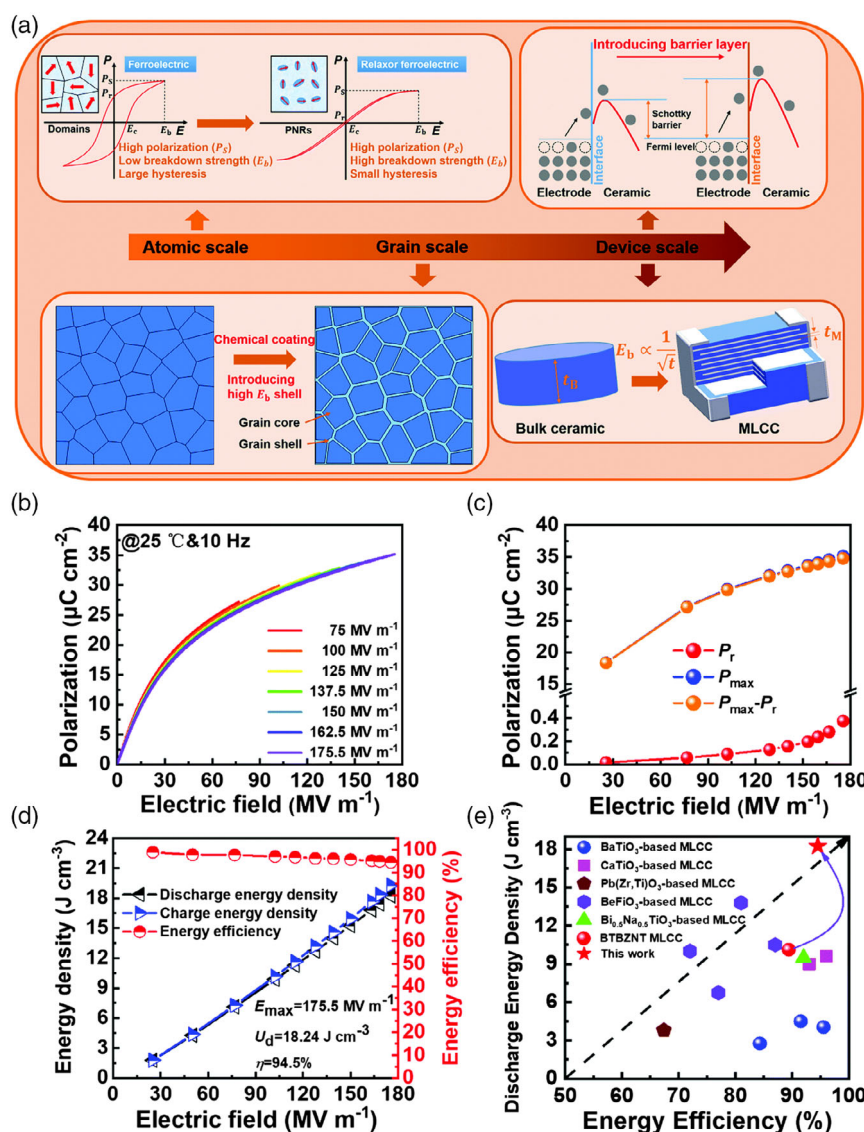


Figure 8. a) Schematic view about multi-scale optimization to realize ultrahigh energy-storage capability for lead-free MLCC. b) Unipolar P-E loops about $0.87\text{BaTiO}_3-0.13\text{Bi}(\text{Zn}_{2/3}(\text{Nb}_{0.85}\text{Ta}_{0.15})_{1/3})\text{O}_3\text{@SiO}_2$ (BTBZNT@SiO₂) MLCCs under 10 Hz. c) The P_r , P_{max} , and $P_{\text{max}}-P_r$ about the BTBZNT@SiO₂ MLCCs with the different imposed electric field. d) Energy density and energy efficiency for the BTBZNT@SiO₂ MLCCs. e) Energy-storage performance comparison for latest reported MLCCs. Reproduced with permission.^[50] Copyright 2020, Royal Society of Chemistry.

large, and the thickness of the dielectric is nanometer, so the capacitance of the supercapacitors is the order of farad (F), higher than the electrolytic capacitors (mF) and dielectric capacitors (μF), which is the reason why it is called “super.”

In 1853, Helmholtz first explored the charge-storage mechanism of capacitors and proposed the electric double layer model in the study of colloidal suspensions.^[52] In 1957, Becker applied for the first patent about an electrochemical capacitor with porous carbon electrodes embedded in a H_2SO_4 solution.^[53] In 1978, Japan’s NEC Corporation commercialized an electrochemical capacitor and called it “supercapacitor.” In 1989, the USA Department of Energy started to support a long-range research on supercapacitors with high energy density, which will be used in electric drive systems and as part of its electric and

hybrid automobile plans.^[54] At present, supercapacitor corporations from all over the world including Maxwell (USA), Nesscap (Korea), ELTON (Russia), and Nippon Chemicon (Japan) have developed and provided different types of supercapacitors and started commercial applications.^[55]

3.2. Classification and Charge-Storage Mechanism of Supercapacitors

Depending on the charge-storage mechanism of electrode materials, supercapacitors enable to be separated into electric double layer capacitors (EDLCs) and PCs.^[56] As shown in Figure 10a, EDLCs accumulate charge mainly by ion adsorption and desorption, and the whole process occurs on the electric double layer of

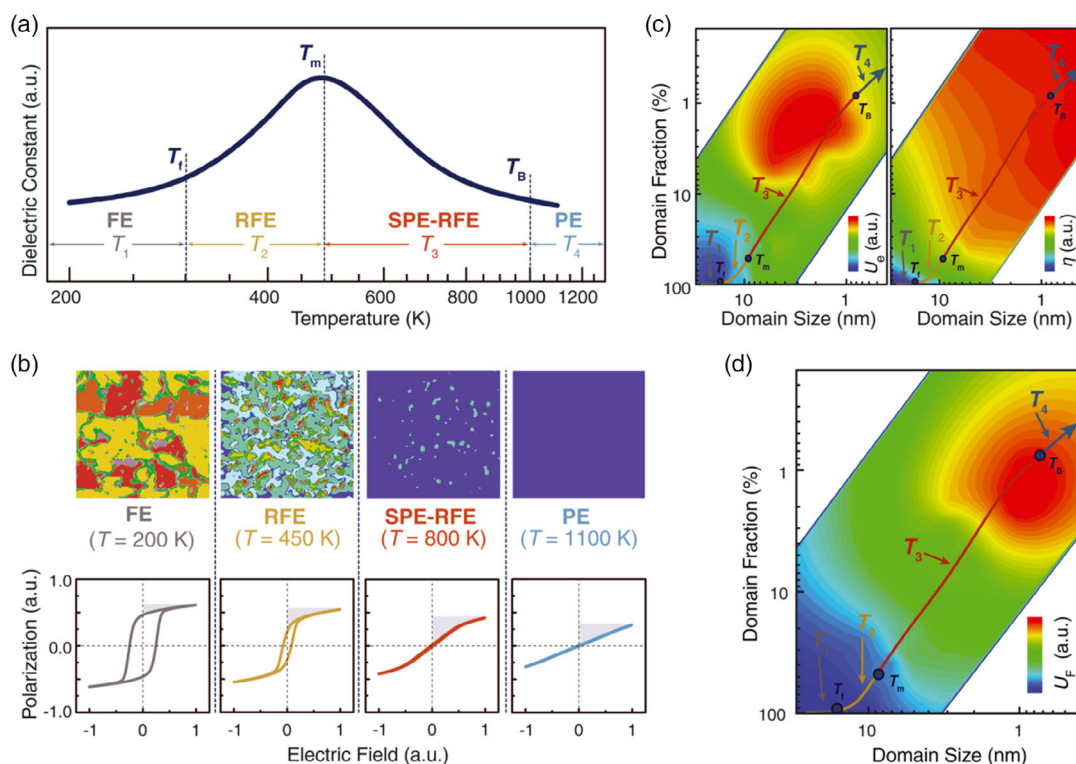


Figure 9. Phase-field simulations of the superparaelectric (SPE) design in relaxor ferroelectrics (RFEs) for high-performance dielectric energy storage. a) Simulated temperature-dependent dielectric constant of the RFE with a composition of 10 mol% Sm-doped yBFO-(1-y)BTO (Sm-BFBT; $\gamma = 0.3$). T1–T4 are the temperature segments divided by the characteristic T_f and T_B values. a.u.: arbitrary units. b) Simulations of the domain structures and P–E loops at 200, 450, 800, and 1100 K of Sm-BFBT with $\gamma = 0.3$, showing FE, conventional RFE, SPE-RFE, and paraelectric (PE) features, respectively. The simulation size is 128 nm by 128 nm by 16 nm. The blue area represents the nonpolar phase; other colored areas indicate domains with various polarization directions. The shaded areas in the P–E loops represent the energy density. c,d) Simulated 2D distributions of (c) the energy density U_e and efficiency η and (d) the U_F parameter of Sm-BFBT for domain size and fraction. The upper-left and lower-right blank areas are thermodynamically unstable regions where data are not collected. The arrowed curve shows the temperature-dependent evolution of Sm-BFBT with $\gamma = 0.3$. Reproduced with permission.^[51] Copyright 2021, American Association for the Advancement of Science.

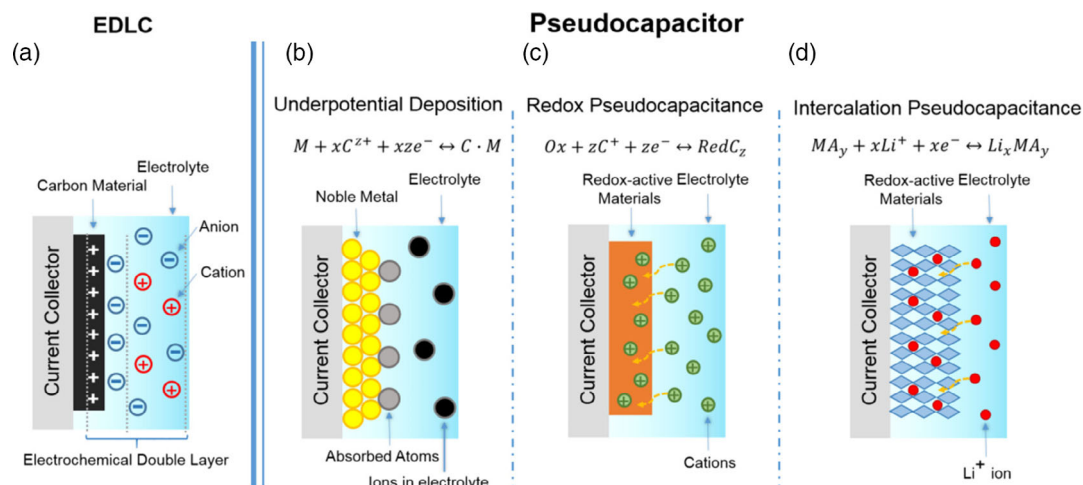


Figure 10. Schematic diagram about charge-storage mechanisms of supercapacitors. a) An electric double layer capacitors (EDLC). Various kinds of pseudocapacitive materials: b) underpotential deposition, c) redox pseudocapacitor, and d) ion intercalation pseudocapacitor. Reproduced with permission.^[2] Copyright 2018, American Chemical Society.

the interface around the electrode and electrolyte.^[57] Since the whole procedure is only a physical variation, no chemical reaction occurs. Therefore, the EDLCs have a high-power density and long durability, but the relatively inferior specific capacitance hinders its wide application. Conway proposed several Faraday mechanisms that can lead to capacitive electrochemical characteristics^[58]: 1) underpotential deposition. When metal ions form an adsorption monolayer on the surface of another metal with a strong interaction that is much higher than its oxidation–reduction potential, deposition under insufficient potential will occur (Figure 10b). A classic example of underpotential deposition is Pb on the surface of Au electrodes^[59]; 2) Redox pseudocapacitance: redox pseudocapacitance is the electrochemical adsorption of ions to the surface or near surface of the electrode material and is accompanied by faraday charge transfer (Figure 10c). RuO₂ is the most typical redox pseudocapacitance material^[60]; 3) Intercalation pseudocapacitance: intercalation pseudocapacitance is the intercalation of ions into the tunnels or interlayers of redox active materials, and there is no crystalline phase transition accompanied by faraday charge transfer (Figure 10d). Nb₂O₅ is a common intercalation pseudocapacitance material.^[61] Furthermore, we utilized the intercalation reaction mechanism of Li-ion battery to elucidate the difference in charge storage between supercapacitors and batteries. In Li-ion batteries, the charge storage mostly depended on the intercalation/deintercalation of Li⁺ within the crystalline structure of electrode materials, coupled with the redox reactions of metal ions within the crystalline structure, which was controlled by the Li⁺ diffusion within a crystalline framework. In contrast, the charge storage of supercapacitors mainly derived from the surface reaction of electrode materials including electrochemical adsorption/desorption of cations and anions at the electrode/electrolyte interface and surface fast faradic redox reactions, which was not limited by the diffusion process.

3.3. Electrode Materials for Supercapacitors

3.3.1. Carbon Materials

Currently, carbon-based materials, conducting polymers, and transition metal oxides/hydroxides are considered to be three major types of electrode materials for supercapacitors. Carbon materials are the electrode materials with industrialization prospects. They possess the merits of abundant natural reserves, low price, convenient processing, non-poison, large specific surface area, excellent conductivity, strong chemical stability, and broad working temperature range.^[62] Generally, the charge storage of carbon materials mainly occurs in the electric double layer of the interface around the electrode and the electrolyte, instead of in the body of electrode material. Thus, the capacitance value mainly is relevant to the surface area that the electrolyte ions could access. The activated carbon (AC), carbon aerogel, carbon nanotubes, and graphene possess the high surface area, which have been widely used in EDLCs.^[63,64] However, in the latest studies, it has been discovered that the surface area of carbon materials is not the only factor that affects the specific capacitance,^[65] since not all the micropores on the electrode can be accessed by electrolyte ions. Therefore, designing carbon materials with a high surface area and optimal pore diameter

distribution is normally applied to moderate the properties of EDLCs. In addition, carbon materials used in supercapacitors exhibit the advantages of protruding power density and durable service life, while their relatively lower specific capacitance and energy density limit their wider applications. The introduction of surface functional groups and heteroatom doping are two important ways to ameliorate the electrochemical performance of carbon materials. In the latest research, Wei et al. successfully constructed the N,O-codoped egg-box-like carbons (EBCs) from coal tar pitch using the less harmful method.^[66] The as-prepared EBCs presented a high specific surface area of 854 m² g^{−1} and exhibited an areal capacitance of 39.8 μF cm^{−2} (340 F g^{−1}) at 0.106 mA cm^{−2}. Furthermore, the manufactured all solid-state supercapacitor achieved a high areal capacitance of 25.0 μF cm^{−2} and an energy density of 0.0233 mWh cm^{−2}. Wang et al. synthesized the modified O-functionalized carbon fiber by employing two-step protonic acid catalysis method (PPOCF), which largely preserved the integrity of the sp² carbon network with abundant reactive O-functional groups embedded in the graphitic carbon host.^[67] When used as the flexible electrode of supercapacitors, the PPOCF delivered a high areal capacitance of 2580 mF cm^{−2} (230 F g^{−1}) at 1 mA cm^{−2} and still maintained 79.1% capacitance retention at 50 mA cm^{−2}. Moreover, the as-assembled symmetric supercapacitor performed an areal capacitance of 1127 mF cm^{−2} at 1 mA cm^{−2} and an energy density of 0.2 mWh cm^{−2} at 0.58 mW cm^{−2}. In Zhang's work, the high density and nitrogen-doped porous carbons (DNPCs) was obtained by the low-temperature pyrolysis of phytic acid (PA)-doped PANI coated on graphene.^[68] The DNPCs electrode performed a high-volumetric capacitance of 643.7 F cm^{−3} (396.9 F g^{−1}) at 0.5 A g^{−1} and the constructed symmetric supercapacitor achieved a high volumetric energy density of 14.6 Wh L^{−1} under the power density of 79.8 kW L^{−1}. Liu et al. successfully constructed the N/O dual-doped carbon spheres with wrinkled nanocages (NOCN) by utilizing dendritic fibrous nanosilica, glucose, and melamine as a sacrificial solid template, carbon source, and nitrogen source, respectively.^[69] The as-prepared NOCN presented a high specific surface area as 813 m² g^{−1} and exhibited a specific capacitance with 311.1 F g^{−1} under 0.5 A g^{−1} and prominent cycle durability of 97.6% capacitance preservation over 10 000 cycles under 10 A g^{−1}. Moreover, the manufactured symmetric supercapacitor achieved an energy density as 12.3 Wh kg^{−1} under 175 W kg^{−1}. Li et al. synthesized the N-doped carbon nanotubes (CNTs) @corncob mesoporous carbon (CNNTs@CMC) composite via employing the waste biomass corncob and melamine as carbon source and nitrogen source, respectively (Figure 11a–d).^[70] The as-prepared symmetric supercapacitors delivered a specific capacitance as 538 F g^{−1} in Na₂SO₄ solution and 320 F g^{−1} with an energy density of 102.5 Wh kg^{−1} under 1 A g^{−1} in LiFePO₆ organic solution (Figure 11e,f).

In Sim's work, the F-doped graphene oxide (FGO) was elaborately fabricated via direct plasma treatment for graphene oxide (GO) (Figure 12a).^[71] The density functional theory calculation was utilized to verify the improved energy-storage capability for the FGO electrodes, which can understand the energy-storage mechanism in depth via the adsorption energy about K⁺ and OH[−] on FGO and the number of charge accumulation (Figure 12b). Meanwhile, the as-constructed symmetric

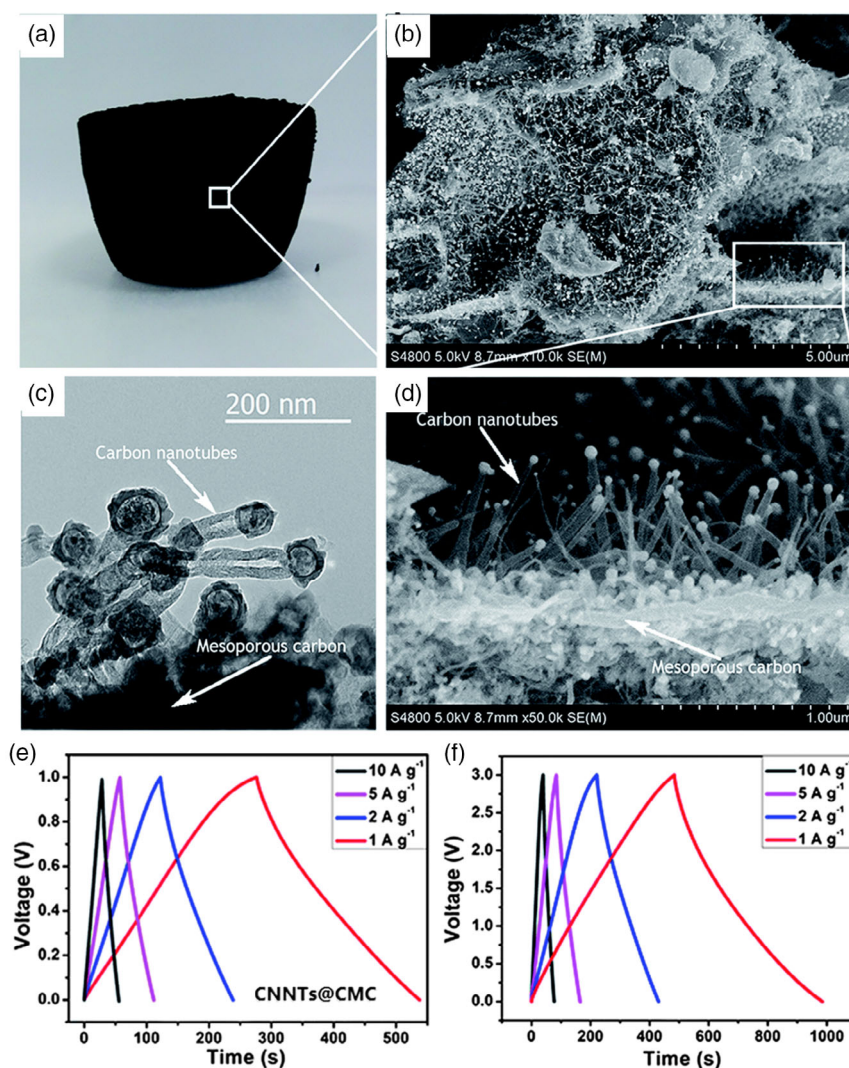


Figure 11. Morphologies of the N-doped CNTs@corn cob mesoporous carbon (CNNTs@CMC) composite material for a) digital ph. b) SEM image. c) Transmission electron microscope (TEM) image. d) Magnified SEM image. GCD profiles under diverse current densities about CNNTs@CMC for e) 1 M Na_2SO_4 electrolyte. f) The 1 M LiPF_6 electrolyte. Reproduced with permission.^[70] Copyright 2017, Royal Society of Chemistry.

supercapacitor delivered the maximum power density as 3200 W kg^{-1} and energy density of 25.87 Wh kg^{-1} and outstanding cycling durability without capacitance loss after 20 000 cycles (Figure 12c,d). In Li's work, they successfully designed the free-standing graphene laminate films with adjustable interlayer distance, and the size of slit pores was exactly modulated.^[72] Benefiting from the very good matching of pore size and electrolyte ions, the film attained a considerably high areal capacitance to $47 \mu\text{F cm}^{-2}$, a gravimetric capacitance of 231 F g^{-1} , and a volumetric capacitance of 203 F cm^{-3} . Furthermore, the constructed symmetric supercapacitor exhibited a volumetric specific energy of 88.1 Wh L^{-1} under an ionic liquid electrolyte.

3.3.2. Conductive Polymers

Conductive polymers have the unique merits of low price, high storage capacity, environmental friendliness, and controllable

redox activity, and are very suitable for electrode materials of supercapacitors.^[73] The conductive polymers is a typical pseudocapacitance electrode material, which stores charge via a reversible redox reaction. When oxidation occurs, ions are transmitted to the polymer backbone; while reduction happens, ions are released from the backbone into the electrolyte. These redox reactions in the conductive polymers will spread over the entire body, not just on the surface. Since the charge and discharge reaction does not involve a phase change, the process is highly reversible. Polyaniline and polypyrrole and their derivatives are commonly used conductive polymers for supercapacitors. For example, Pan et al. used phytic acid (a rich natural product found in plants) as a gelling agent and direct dopant to form a polyaniline (PANI) hydrogel network without insulating polymers.^[74] The prepared PANI hydrogel had a specific capacitance as 480 F g^{-1} under 0.2 A g^{-1} . Huang et al. attained polypyrrole nanowire arrays through a simple electrochemical polymerization process.^[75]

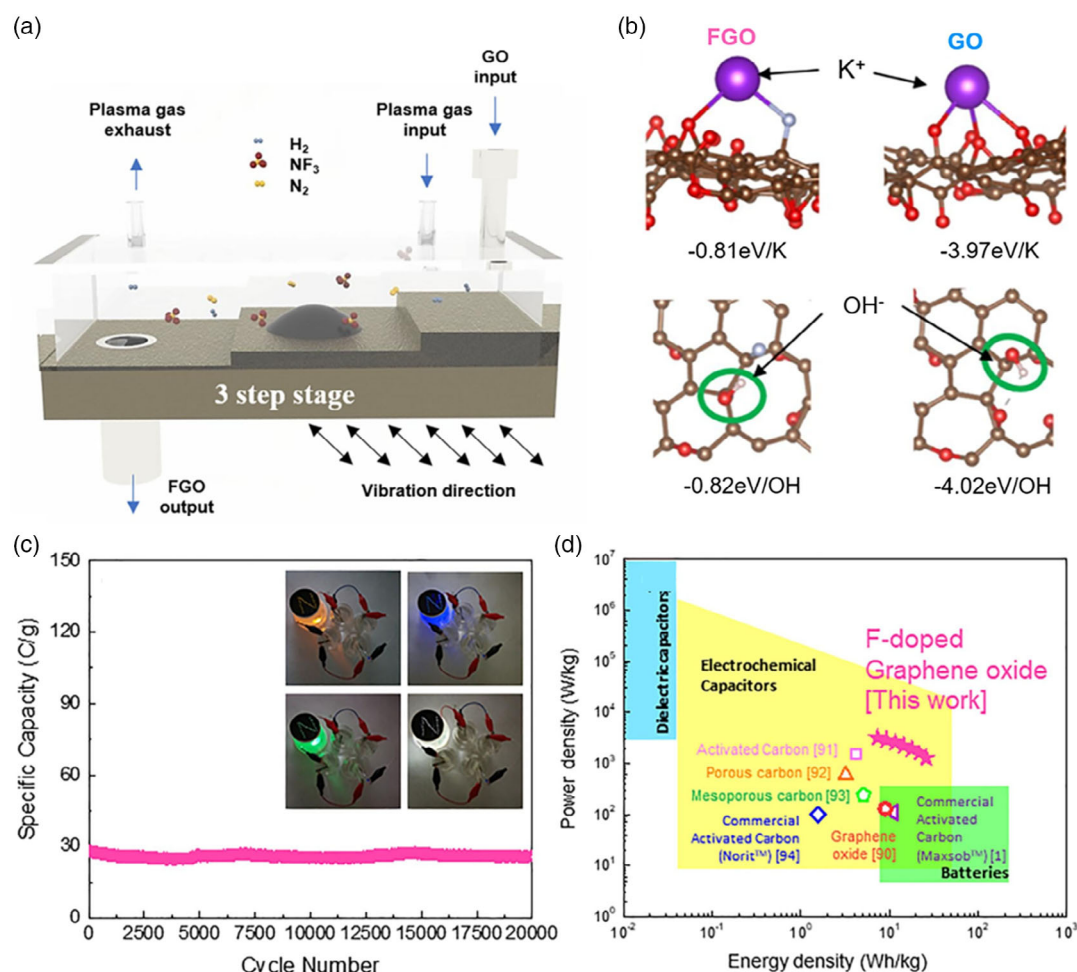


Figure 12. a) Schematic diagram about the synthesis of F-doped graphene oxide (FGO). b) K⁺ and OH⁻ adsorption energies on FGO and graphene oxide (GO). c) The cycling performance about the FGO//FGO symmetric supercapacitor. The illustration displays digital images about the light-emitting diodes (LEDs) measured with the FGO//FGO symmetric supercapacitors. d) Ragone plot of FGO//FGO symmetric supercapacitors. Reproduced with permission.^[71] Copyright 2022, Elsevier.

The polypyrrole nanowire arrays possessed a high specific capacitance as 566 F g⁻¹ under 1.1 A g⁻¹. At the same time, the specific capacitance decayed to 70% of the initial value after 300 cycles under 1.1 A g⁻¹. Wang et al. deposited the 1D PANI nanowires on the carbon framework (CF-PANI) through a facile electrodeposition strategy.^[76] The CF-PANI electrode achieved a high mass loading of 21.3 mg cm⁻³, a gravimetric capacitance of 866 F g⁻¹, and volumetric capacitance of 18.5 F cm⁻³. Furthermore, an asymmetric supercapacitor (ASC) assembled with CF-PANI anode and carbon framework cathode delivered a high energy density of 44 Wh kg⁻¹ at 800 W kg⁻¹. Although the conductive polymers show a high specific capacitance, its poor cycling durability limits its wide application. This inferior cycling stability is due to the unstable chemical structure of the conductive polymers and the slow charge-transfer rate. Generally, the structure of the conductive polymers undergoes expansion and contraction during charging and discharging, resulting in a poor cycle performance of the conductive polymers. In addition, the bulk material of the

conductive polymers has a dense structure, which will hinder the penetration of electrolyte ions, making it difficult to obtain excellent electrochemical performance. Therefore, the combination of conductive polymers and other materials (including carbon materials, inorganic metal oxides/hydroxides) has been utilized to enhance its electrochemical capability. For example, Wang et al. prepared the nanofibrillar polymer poly(3,4-ethylenedioxythiophene) (PEDOT) with a high mass loading of 30.2 mg cm⁻² by employing the α-Fe₂O₃ particles as an oxidant precursor.^[77] The as-obtained flexible PEDOT electrode performed a gravimetric capacitance of 206 F g⁻¹, an areal capacitance of 6210 mF cm⁻², and a volumetric capacitance of 138 F cm⁻³ at 2 mV s⁻¹. The PEDOT symmetric supercapacitor behaved an areal capacitance of 2243 mF cm⁻² and an energy density of 312 μWh cm⁻². Das et al. successfully grew the CuS@PEDOT on the flexible conductive carbon cloth (CC/CuS@PEDOT) by combining solvothermal and potentiostatic electrodeposition methods, which accomplished the prominent improvement of areal capacity and cycling stability.^[78] Moreover, a quasi-solid-

state ASC derived from the CC/CuS@PEDOT as negative electrode and CC/Co-V-Se as positive electrode attained an areal capacity as $0.331 \text{ mAh cm}^{-2}$ under 1 mA cm^{-2} and achieved a maximum volumetric energy density of 2.21 mWh cm^{-3} and outstanding cycling durability (Figure 13a–d). Two quasi-solid-state ASCs in series could light up the LEDs and successfully power a small motor fan (Figure 13e). To settle with the poor cycling stability of PANI, Chang et al. grafted the 4-azidotetrafluorobenzoyl tetraaniline on 3D graphene networks (ATgGN) via a simple solvothermal self-assembly method.^[79] The ATgGN electrode exhibited a gravimetric capacitance of 278 F g^{-1} at 1 A g^{-1} and an areal capacitance of 135 mF cm^{-2} at 1 mA cm^{-2} . The fabricated symmetric all-solid-state supercapacitors represented the remarkable cycling life with 87% capacitance retention after 30 000 cycles. In Wang's work, the PANI nanoparticles were inserted into MXene interlayers to obtain $\text{Ti}_3\text{C}_2/\text{PANI}$ composite via the self-assembly approach.^[80] The $\text{Ti}_3\text{C}_2/\text{PANI}$ electrode

exhibited superior capacitances of 377 F g^{-1} , 873 F cm^{-3} , and 1885 mF cm^{-2} at 1 mV s^{-1} and excellent cycling performance with almost 100% capacitance retention after 10 000 cycles. Moreover, the fabricated symmetric supercapacitor displayed an energy density of $90.3 \text{ } \mu\text{Wh cm}^{-2}$ at 28.1 mW cm^{-2} and a high volumetric energy density of 20.9 Wh L^{-1} .

3.3.3. Metal Oxides

Metal oxides composed of transition metal families store charges through rapid and reversible redox reactions, thus they have a larger specific capacitance than carbon materials and preferable cycling stability than conductive polymers. Therefore, transition metal oxides are very attractive electrode materials for improving the electrochemical capability of supercapacitors. RuO_2 is the first metal oxide used in supercapacitors. The cyclic voltammetry

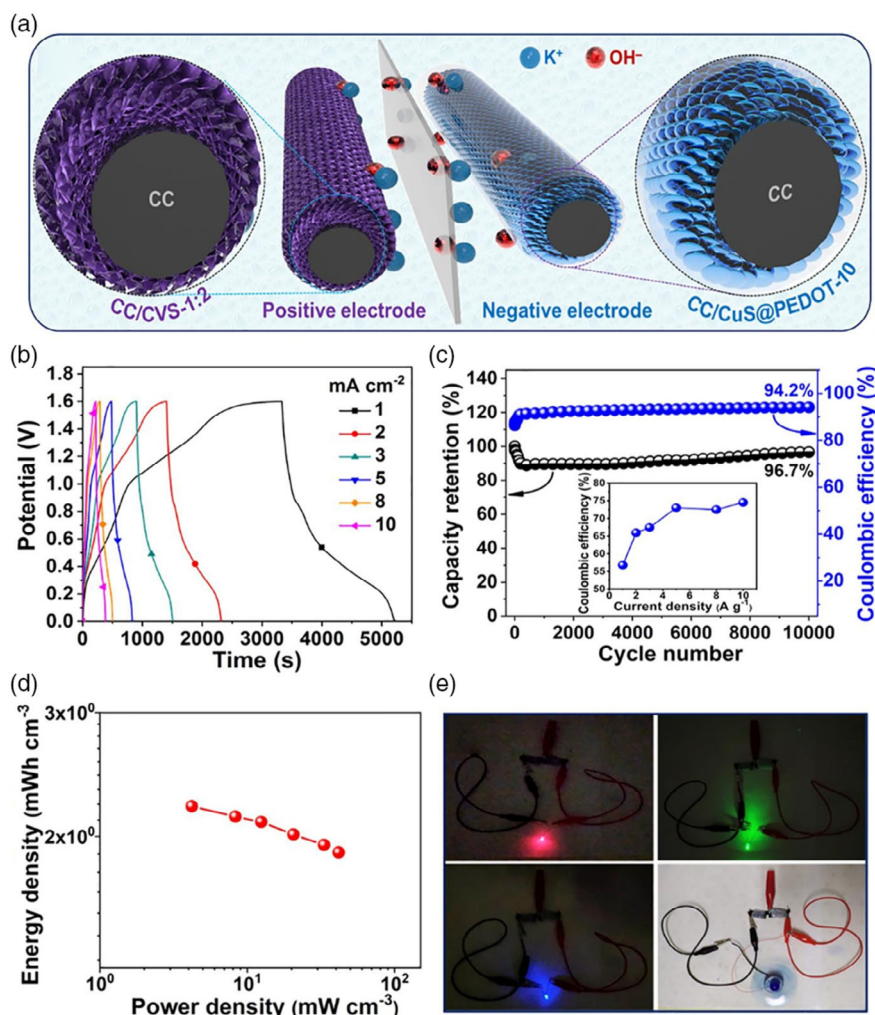


Figure 13. The electrochemical properties of quasi-solid-state asymmetric supercapacitor (ASC) constructed with carbon cloth (CC)/CuS@PEDOT (poly(3,4-ethylenedioxythiophene)) negative electrode and CC/Co-V-Se-positive electrode. a) Schematic diagram of the diffusion of electrolyte ions in quasi-solid-state ASC device in electrochemical reaction. b) GCD profiles about the ASC device under diverse current densities. c) Cycling stability and coulombic efficiency for the ASC device under 5 mA cm^{-2} (illustration exhibits the coulombic efficiency with diverse current density). d) Ragone plot of the ASC device. e) Photos of two ASC devices in series lightening three colors of light-emitting diodes (LEDs) and driving a small electrical motor fan. Reproduced with permission.^[78] Copyright 2022, Elsevier.

(CV) curves of RuO_2 present a rectangular-like shape, and its electrochemical behavior is similar to that of an EDLC, but essentially it stores charge through the faraday redox reaction. As Thierry Brousse proposed, only electrode materials such as RuO_2 and MnO_2 that perform electrochemical behavior similar to that of EDLCs can be called the pseudocapacitive materials.^[81] Although RuO_2 has the merits of high theoretical specific capacitance (1450 F g^{-1} , 0–1.0 V), good thermal and cycling durability, and excellent conductivity, the rare metal ruthenium and high price limit its large-scale application.^[82] To overcome this dilemma, people have paid more attention to the research of replacing RuO_2 with low-cost transition metal oxides for supercapacitors.

In recent years, many documents have incorrectly regarded electrode materials with battery-like electrochemical behavior as pseudocapacitive materials. Accordingly, the proposal of emerging battery-type electrode materials better prevents misleading new electrochemical scholars.^[83] The battery-type electrode materials may undergo phase changes during charging and discharging, and their electrochemical processes are affected by ion diffusion.^[84] Compared with pseudocapacitance electrode

materials, the battery-type electrode materials present a pair of distinct redox peaks in the CV curves, and display a nonlinear curve with potential platform in the galvanostatic charge/discharge (GCD) profiles. Therefore, the battery-type electrode materials generally behave very large specific capacity, while poor rate capability resulted from slow kinetics. Due to their variable metal valence and rich redox reactions, transition-metal oxides containing NiO ,^[85] NiCo_2O_4 ,^[86] Co_3O_4 ,^[87] CuCo_2O_4 ,^[88] Fe_2O_3 ,^[89] NiFe_2O_4 ,^[90] as the battery-type electrode materials, have been widely used in the research of supercapacitors. For example, in Saleki's work, the double-shell CuCo_2O_4 hollow spheres was constructed by utilizing a metal–organic framework (MOF) as self-template (Figure 14a).^[91] The CuCo_2O_4 hollow spheres electrode attained a high specific capacity as 701 C g^{-1} under 2 A g^{-1} and superior cycle durability with 93.6% capacity preservation over 6000 cycles (Figure 14b). The constructed ASC with CuCo_2O_4 hollow spheres cathode and reduced GO (rGO) anode displayed an energy density as 38.4 Wh kg^{-1} and a power density of 16 kW kg^{-1} . Liao et al. successfully grown the maguery-like CuCo_2O_4 nanowires on nickel foam via a common hydrothermal approach followed by the annealing process.^[92] The

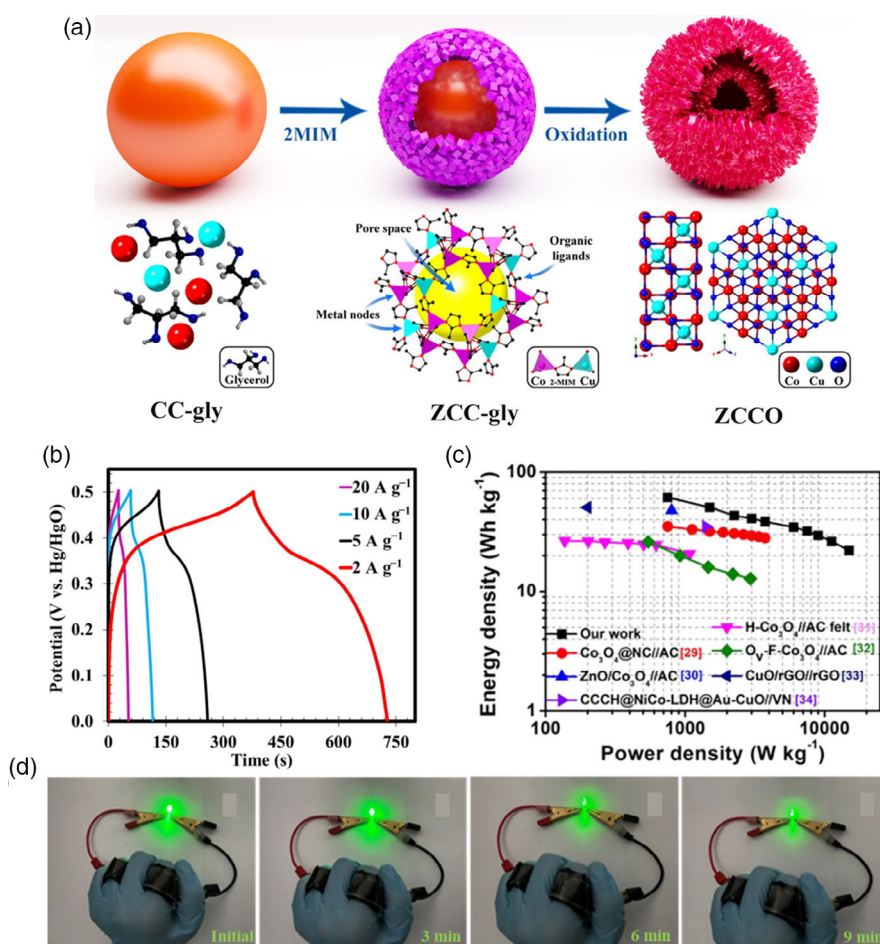


Figure 14. a) Schematic and crystal illustration about double shell CuCo_2O_4 hollow spheres fabrication process. b) GCD profiles for the double shell CuCo_2O_4 hollow spheres under various current densities. Reproduced with permission.^[91] Copyright 2019, Academic Press Inc. c) Ragone plots about $\text{O}_v\text{-Cu-Co}_3\text{O}_4\text{@C//S-rGO}$ ASC and the previously reported ASCs. d) Wearable manifestation as an energy-storage system applying two serially connected devices to light up a green bulb. Reproduced with permission.^[96] Copyright 2021, American Chemical Society.

binder-free CuCo_2O_4 electrode achieved a gravimetric capacitance of 982 F g^{-1} under 1.5 A g^{-1} and an areal capacitance of 3.27 F cm^{-2} at 5 mA cm^{-2} . Meanwhile, the constructed symmetric supercapacitor possessed an energy density of 16.8 Wh kg^{-1} under 513 W kg^{-1} . Mei et al. fabricated the $\text{NiSe}_2/\text{Ni}(\text{OH})_2$ composite materials via a novel epitaxial-like growth approach with NiSe_2 precursor.^[93] The heterojunction composite achieved a high specific capacity as 909 C g^{-1} under 1 A g^{-1} and 597 C g^{-1} under 20 A g^{-1} . The ASC constructed with the $\text{NiSe}_2/\text{Ni}(\text{OH})_2$ cathode and p-phenylenediamine-functional rGO anode delivered a high energy density as 76.1 Wh kg^{-1} under 906 W kg^{-1} and protruding cycle capability with 82% reservation under 8000 cycles at 10 A g^{-1} . In Tong's group, the $\text{NiCo}_2\text{O}_4@\text{Ni}(\text{OH})_2$ was anchored on the 3D nitrogen-doped graphene (TRGN)/carbon nanotubes sponge ($\text{NiCo}_2\text{O}_4@\text{Ni}(\text{OH})_2/\text{TRGN-CNTs-S}$) via the facile hydrothermal and electrodeposition method.^[94] The $\text{NiCo}_2\text{O}_4@\text{Ni}(\text{OH})_2/\text{TRGN-CNTs-S}$ electrode behaved a gravimetric capacitance of 1810 F g^{-1} and a volumetric capacitance of 847.7 F cm^{-3} at 1 A g^{-1} . Patil et al. synthesized the NiCo_2O_4 nanospikes on the rGO-deposited acid-treated carbon fiber ($\text{NiCo}_2\text{O}_4@\text{rGO}/\text{ACF}$) through a facile hydrothermal strategy.^[95] The battery-type $\text{NiCo}_2\text{O}_4@\text{rGO}/\text{ACF}$ electrode gained a specific capacitance of 1487 F g^{-1} (1338 mF cm^{-2}) at 3 mA cm^{-2} . In addition, the assembled hybrid supercapacitor with $\text{NiCo}_2\text{O}_4@\text{rGO}/\text{ACF}$ -positive electrode and $\text{Ti}_3\text{C}_2\text{T}_x/\text{ACF}$ -negative electrode performed a gravimetric energy density of 44.36 Wh kg^{-1} at 985 W kg^{-1} and a volumetric energy density of 0.72 mWh cm^{-3} at 16.13 mW cm^{-3} . Presently, in Liu's work, they successfully incorporated Cu dopants and O deficient into Co_3O_4 nanocrystals blocked in a carbon matrix ($\text{O}_v\text{-Cu-Co}_3\text{O}_4@\text{C}$).^[96] The Cu dopants and O vacancies in $\text{O}_v\text{-Cu-Co}_3\text{O}_4@\text{C}$ corporately manipulated electronic states and afforded more accessible active sites, thereby enhancing conductivity and rich redox activity. Furthermore, a solid-state flexible ASC ($\text{O}_v\text{-Cu-Co}_3\text{O}_4@\text{C}/\text{S-rGO}$ ASC) with $\text{O}_v\text{-Cu-Co}_3\text{O}_4@\text{C}$ cathode and S-doped rGO anode reached an energy density as 64.1 Wh kg^{-1} under 800 W kg^{-1} with superior deformable power-supply capability (Figure 14c,d).

3.3.4. Other Materials

In addition to the aforementioned three electrode materials for supercapacitors, the other emerging materials have also been employed to the research of supercapacitors, such as Mxene, TMDs, and metal phosphide/nitride. For example, in Yang's group, they employed the atomically thin (1–3 nm) 2D $\text{Ti}_3\text{C}_2\text{T}_x$ with a horizontal size about $8 \mu\text{m}$ as aqueous inks for extrusion-based free-standing 3D printing (Figure 15a).^[97] The 3D-printed micro-supercapacitors (MSCs) delivered a high areal capacitance to 2.1 F cm^{-2} under 1.7 mA cm^{-2} and a gravimetric capacitance of 242.5 F g^{-1} under 0.2 A g^{-1} with 90% capacitance reservation after 10 000 cycles (Figure 15b,c). It further exhibited a high energy density as $0.0244 \text{ mWh cm}^{-2}$ and a power density of 0.64 mW cm^{-2} under 4.3 mA cm^{-2} (Figure 15d,e). In addition, they further reported the scalable manufacturing about MXene ($\text{Ti}_3\text{C}_2\text{T}_x$) films up to $700 \mu\text{m}$ thickness via a simple freeze-assisted tape-casting way.^[98] Due to the punctilious quality control steps in the $\text{Ti}_3\text{C}_2\text{T}_x$ peeling process and the vertical

alignment microstructure design of the films, these electrodes displayed a gravimetric and areal specific energy as 2.8 Wh kg^{-1} and $1.8 \mu\text{Wh cm}^{-2}$ for $150 \mu\text{m}$ films and 2.6 Wh kg^{-1} and $11.3 \mu\text{Wh cm}^{-2}$ for $700 \mu\text{m}$ films. They also delivered a gravimetric power density up to 150 kW kg^{-1} under 1000 A g^{-1} and an areal power density of 667 mW cm^{-2} under 4444 mA cm^{-2} ($700 \mu\text{m}$). Meanwhile, there still have been numerous strategies was employed to enhance the electrochemical properties, such as morphology/structure tunable, metal/nonmetal element-doped composites. Owing to the space limitation, their detailed content is not elaborated there.

It worth noticing that many literatures reported very high gravimetric capacitance at quite low mass loading, which was not applicable to the practical applications. Meanwhile, some thin-film electrodes displayed high gravimetric capacitance, but the areal capacitance was very small, which was also not suitable for practical application. Therefore, the mass loading, gravimetric capacitance, volumetric capacitance, and areal capacitance of the electrode for supercapacitors was summarized in the Table 1.

4. Emerging Hybrid Ion Capacitors

With the increasing demand for electric automobile and electronic devices, the requirement for energy-storage systems is becoming more and more stringent. Although the supercapacitors possess protruding power density and brilliant cycle durability, the low energy density has always been a bottleneck and hinders its widely practical applications. To tackle the dilemma, the introduction of emerging capacitors containing metal ion HCs and DICs is expected to increase energy density without deteriorating power density. The metal ion HCs is composed of a battery-type faradaic electrode for energy source and a capacitive electrode for power source.^[99] Based on the valence of the cation charge carriers, the metal-ion HCs enable to be separated into two types: one involves univalent metal-ion HCs, including lithium-ion HCs (LICs), sodium-ion HCs (NICs), and potassium-ion HCs (KICs); the other involves multivalent metal-ion HCs, including zinc-ion HCs (ZICs), magnesium-ion HCs (MICs), calcium-ion HCs (CICs), and aluminum-ion HCs (AICs).^[100] The development history of metal-ion HCs was illustrated in Figure 16. Since 2001, Amatucci and colleagues established the first LIC through utilizing AC and nanostructured $\text{Li}_4\text{Ti}_5\text{O}_{12}$ (LTO) as the cathode and anode, respectively.^[101] Soon afterward, the corresponding metal-ion HCs were successively reported. In 2012, Chen et al. reported the first NIC based on a hierarchically porous nanowire composite.^[102] In 2017, Azais's group assembled the first KIC with the active carbon-positive electrode and graphite-negative electrode.^[103] In 2016, Tian et al. proposed the first ZIC, which was composed of an oxidized carbon nanotubes cathode and a zinc anode in an aqueous ZnSO_4 electrolyte.^[104]

4.1. Electrode Materials for Metal-Ion HCs

As we mentioned, electrode materials are the critical part that determine the electrochemical capability of EES devices, and it has no exception for the metal-ion HCs. As the anode materials

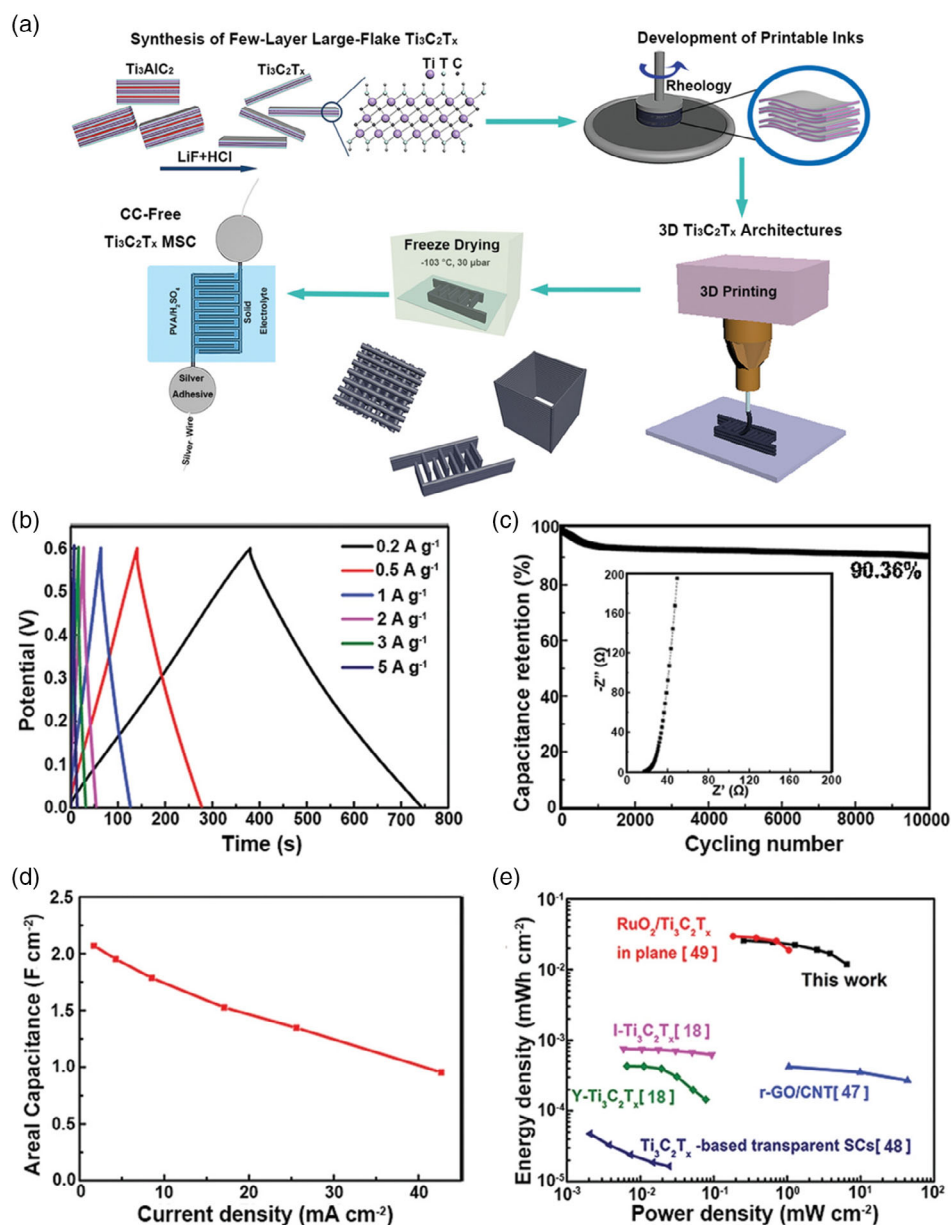


Figure 15. a) Schematic diagram about the fabricated method of free-standing 3D printing MXene architectures and micro-supercapacitors (MSCs) demonstrator. Electrochemical capability of 3D-printing few-layer large-flake $\text{Ti}_3\text{C}_2\text{T}_x$ interdigital electrodes integrated into symmetric MSCs without current collector. b) GCD profiles under different current densities. c) Cycling stability test. d) Areal capacitance with various areal current densities. e) Ragone plots about the 3D-printing $\text{Ti}_3\text{C}_2\text{T}_x$ supercapacitors compared with other literature. Reproduced with permission.^[97] Copyright 2019, Wiley-Blackwell.

of metal-ion HCs, it should be liable to form capacitance on the electrode–electrolyte interface to raise the chemical and mechanical stability. At present, carbon materials, metal oxides, TMDs, MXenes, and alloys are the common anode materials of metal-ion HCs. Intriguingly, the Zn and Mg metal enable to be directly employed as anode for the ZICs and MICs, while the alkali metals (Li, Na, and K) are not suitable for anode owing to their activity and dendrite growth. The cathodes of metal-ion HCs need to possess high specific surface area and superb conductivity, which is beneficial to the fast adsorption/desorption process, such as AC, metal oxides, and MXenes. Each material has its own

advantages and disadvantages, and it is still under further research and improvement. In this following, we briefly describe the progress of electrode materials in metal-ion HCs.

4.1.1. Carbon Materials

Carbon materials are massively applied to one kind of intercalation anode materials in HCs by virtue of their lower price, abundant reserve, chemical stability, high conductivity, and tunable pore structure.^[105] Among them, the CNTs and graphene as the most representative carbon materials have inspired the great

Table 1. The mass loading, gravimetric capacitance, volumetric capacitance, and areal capacitance of the electrode for supercapacitors.

| Material ^{a)} | Mass loading | Gravimetric capacitance | Volumetric capacitance | Areal capacitance | Reference |
|--|-----------------------------|--|---|---|-----------|
| N,O-codoped egg-box-like carbons | 2.15 mg cm ⁻² | 340 F g ⁻¹ at 0.106 mA cm ⁻² | / | 39.8 μF cm ⁻² at 0.106 mA cm ⁻² | [66] |
| O-functionalized carbon fibers | 11.2 mg cm ⁻² | 230 F g ⁻¹ at 1 mA cm ⁻² | / | 2580 mF cm ⁻² at 1 mA cm ⁻² | [67] |
| Nitrogen-doped porous carbon | 2–2.5 mg cm ⁻² | 396.9 F g ⁻¹ at 0.5 A g ⁻¹ | 643.7 F cm ⁻³ at 0.5 A g ⁻¹ | / | [68] |
| Graphene-laminated film | 1 mg cm ⁻² | 230 F g ⁻¹ at 1 mA cm ⁻² | 203 F cm ⁻³ at 1 mA cm ⁻² | 47 μF cm ⁻² at 0.106 mA cm ⁻² | [72] |
| Polyaniline nanowires | 21.3 mg cm ⁻³ | 866 F g ⁻¹ at 2 mV s ⁻¹ | 18.5 F cm ⁻³ at 2 mV s ⁻¹ | / | [76] |
| α-Fe ₂ O ₃ -derived PEDOT | 30.2 mg cm ⁻² | 206 F g ⁻¹ at 2 mV s ⁻¹ | 138 F cm ⁻³ at 2 mV s ⁻¹ | 6210 mF cm ⁻² at 2 mV s ⁻¹ | [77] |
| ATgCN | 0.3–0.5 mg cm ⁻² | 278 F g ⁻¹ at 1 A g ⁻¹ | / | 135 mF cm ⁻² at 1 mA cm ⁻² | [79] |
| Ti ₃ C ₂ /PANI | 5 mg cm ⁻² | 377 F g ⁻¹ at 1 mV s ⁻¹ | 873 F cm ⁻³ at 1 mV s ⁻¹ | 1885 mF cm ⁻² at 1 mV s ⁻¹ | [80] |
| Maguery-like CuCo ₂ O ₄ /Ni foam | 3.3 mg cm ⁻² | 982 F g ⁻¹ at 1.5 A g ⁻¹ | / | 3.27 F cm ⁻² at 5 mA cm ⁻² | [92] |
| NiCo ₂ O ₄ @Ni(OH) ₂ /TRGN-CNTs-S | 0.8 mg cm ⁻³ | 1810 F g ⁻¹ at 1 A g ⁻¹ | 847.7 F cm ⁻³ at 1 A g ⁻¹ | / | [94] |
| NiCo ₂ O ₄ @ rGO/ACF | 1.12 mg cm ⁻² | 1487 F g ⁻¹ at 3 mA cm ⁻² | / | 1338 mF cm ⁻² at 3 mA cm ⁻² | [95] |
| Ti ₃ C ₂ T _x | 8.5 mg cm ⁻² | 242.5 F g ⁻¹ at 0.2 A g ⁻¹ | / | 2.1 F cm ⁻² at 1.7 mA cm ⁻² | [97] |

^{a)} PEDOT: poly(3,4-ethylenedioxythiophene); PANI: polyaniline; rGO: reduced graphene oxide; ACF: acid-treated carbon fiber.

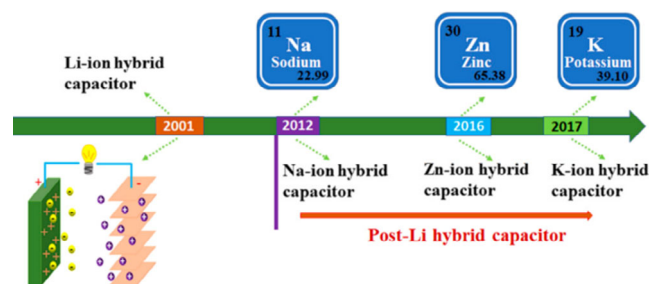


Figure 16. Historical timeline for metal-ion hybrid capacitors (HCs). Reproduced with permission.^[100] Copyright 2021, Elsevier BV.

research enthusiasm. Taking into account the low specific surface area, inferior specific capacity and poor pore distribution for CNTs, the improvement of CNTs became the research hot-spots, including the element doping and grafting of metal oxides. For example, in Que's study, the elastic oxygen-vacancy TiO_{2-x}/CNT composite film was successfully fabricated, which possessed the rapid electron/ion-transmission network and behaved the extraordinary electrochemical performance when used as the self-supported and light-weight anode of metal-ion HCs.^[106] Luan and colleagues successfully engineered a nitrogen and phosphorus codoped multilayer graphene (NPG) material via an arc discharge method utilizing (NH₄)₃PO₄ as nitrogen and phosphorus source (Figure 17a–c).^[107] Furthermore, the whole carbon-based LICs and KICs were constructed utilizing the synthesized NPG as anode and AC as cathode, which achieved maximum energy densities up to 195 and 104.4 Wh kg⁻¹ and power densities up to 14983.7 and 14 976 W kg⁻¹, respectively (Figure 17d,e).

4.1.2. Metal Oxides

In the past, several metal oxides with the different charge-storage mechanism have been reported as the attractive anode materials of HCs due to their improved specific capacity and energy

density, including pseudocapacitance (RuO₂), intercalation (TiO₂), and conversion (Fe₃O₄ and MoO₃).^[108] These metal oxides exhibit high specific capacity and energy density, but the inferior conductivity and weak structural stability restrict their widely application. Therefore, the combination of metal oxides and carbonaceous materials is employed to increase the electrochemical capability. For example, Huo and colleagues cleverly designed the *P*-doping TiO₂/*P*-doping carbon nanofibers (PTO/PC NFs) by employing a convenient electrospinning mean using Na₂HPO₄ as a phosphorus source (Figure 18a).^[109] The constructed AC//PTO/PC LICs with PTO/PC NFs anode and AC cathode presented a high energy density as 72 Wh kg⁻¹ at 250 W kg⁻¹ (Figure 18b). The *P*-doped in TiO₂ nanoparticles and C-coated on the surface enable to ameliorate the conductivity of TiO₂ nanoparticles. Furthermore, the surface-coated C can effectively promote the structural stability of TiO₂. Recently, in Liang's work, the porous CoV₂O₆ nanosphere@GO composites (CoV₂O₆@GO) was successfully acquired via a facile solvothermal method and first used as the anode material for PICs.^[110] The CoV₂O₆@GO composites displayed an initial high discharge capacity up to 264 mAh g⁻¹ under 1 A g⁻¹ and superior rate capability of 97 mAh g⁻¹ under 10 A g⁻¹. Furthermore, a PIC coupling with CoV₂O₆@GO anode and AC cathode acquired a high energy density to 150.8 and 78.2 Wh kg⁻¹ under 112.5 and 22 500 W kg⁻¹ as well as conspicuous cycling performance with 96.8% reservation over 3000 cycles under 1 A g⁻¹.

4.1.3. TMDs

The most TMDs are also the very intriguing anode materials of HCs owing to their 2D structure, atomic thickness, low price, and environmental friendliness, such as Ni₃S₂, SnS₂, MoS₂, FeSe₂, CoSe₂, and MoSe₂.^[108] Remarkably, the ion-storage mechanism of most 2D TMDs with metal ions is somewhat similar to the intercalation/deintercalation mechanism of insertion-type materials and the conversion mechanism of conversion-type materials.^[111] Presently, the research of TMDs is committed

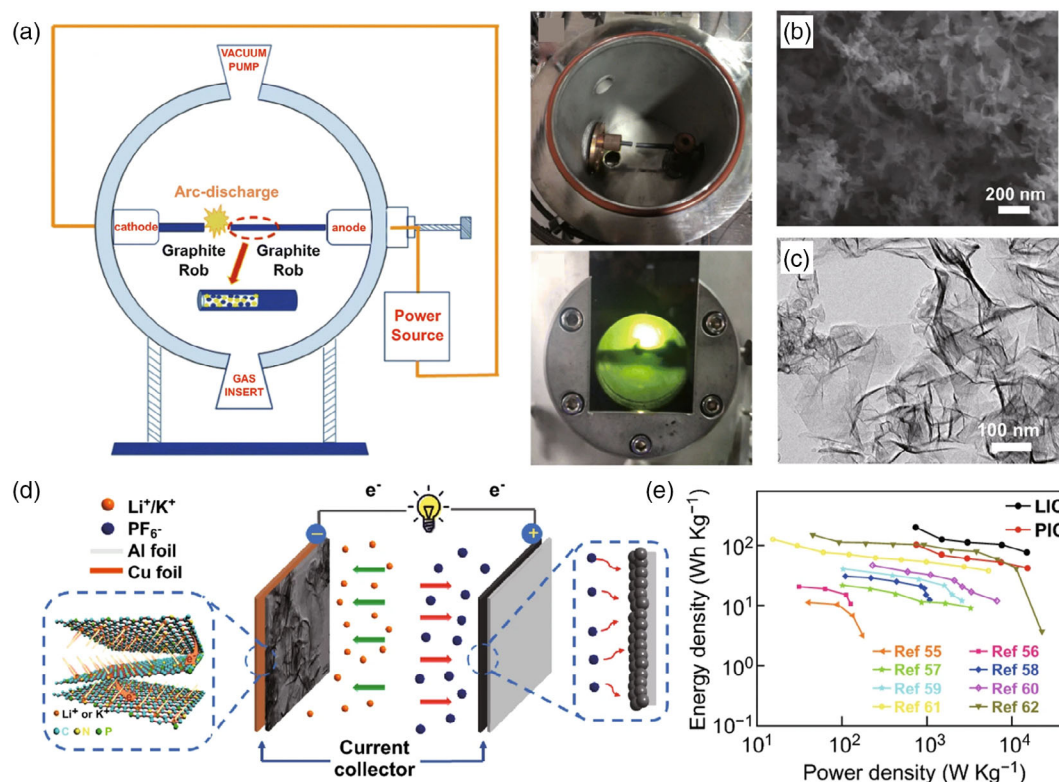


Figure 17. a) Schematic presentation about the arc discharge method and digital photo. b) SEM and c) TEM images about NPG nanosheets. d) Schematic diagram about the working mechanism. e) Ragone plots compared with literature values under the optimized cathode/anode mass ratio. Reproduced with permission.^[107] Copyright 2019, Springer Singapore.

to raise the electrical conductivity and expand the interlayer space. For example, Sarkar and co-worker successfully grown the 3D free-standing MoS_2/rGO hybrid nanoflakes on Mo foils by employing a hydrothermal approach with thiourea as sulfur source and exfoliating agent.^[112] Intercalation of NH_4^+ into MoS_2 extended the interlayer spacing to 0.95 nm, which was beneficial to the Na^+ -ion insertion/deinsertion (Figure 18c). Meanwhile, the addition of rGO also extended electronic conductivity of the hybrid material. Therefore, the assembled supercapacitor ($\text{MoS}_2/\text{rGO}/\text{Fe}_2\text{O}_3/\text{MnO}_2$ ASC) with MoS_2/rGO as anode and $\text{Fe}_2\text{O}_3/\text{MnO}_2$ as cathode attained a volumetric energy density to 0.78 mWh cm^{-3} and compelling cycling performance of 98% reservation over 20 000 cycles (Figure 18d,e). Ge et al. fabricated the N-doping carbon-coated FeSe_2 clusters ($\text{FeSe}_2/\text{N-C}$) via a solvothermal route.^[113] The $\text{FeSe}_2/\text{N-C}$ exhibited a capacity value of 295 mAh g^{-1} under 100 mA g^{-1} during 100 cycles and a high rate capability as 158 mAh g^{-1} under 2000 mA g^{-1} after 2000 cycles. The as-constructed potassium-ion HC with AC cathode and $\text{FeSe}_2/\text{N-C}$ anode achieved a high energy density of 230 Wh kg^{-1} and a power density of 920 W kg^{-1} .

4.1.4. MXene

MXene has raised intensively concern because of its adjustable interlayer spacing, high volumetric capacitance, hydrophilicity, and remarkable conductivity. At the moment, people have engineered diverse MXene materials exceeding 20 kinds, and its

representative members mainly include Ti_3C_2 , Ti_2C , V_2C , Nb_4C_3 , etc.^[114] The current research on MXene is focused on suppressing irreversible agglomerations caused by strong van der Waals interaction between layers, which can induce underutilization of the surface groups and is harmful to charge storage. For example, in Luo's work, the S element was successfully intercalated into interlayer of the cetyltrimethylammonium bromide-pretreated Ti_3C_2 ($\text{CT-S@Ti}_3\text{C}_2$) and the interlayer spacing was expanded by the Ti-S bond (Figure 19a).^[115] The $\text{CT-S@Ti}_3\text{C}_2$ electrode performed the superior Na-ion-storage ability with a capacity of 550 mAh g^{-1} under 0.1 A g^{-1} and protruding rate ability with 120 mAh g^{-1} under 15 A g^{-1} . The assembled NICs-coupled $\text{CT-S@Ti}_3\text{C}_2$ anode with AC cathode behaved an energy density up to $114.03 \text{ Wh kg}^{-1}$ under 237 W kg^{-1} . Liu et al. reported the *P*-phenylenediamine was electrostatically intercalated into Nb_2CT_x layers ($\text{PPDA-Nb}_2\text{CT}_x$), which not only endowed the increased interlayer distance to promote the Li^+ diffusion, but also improved layered structure stability attributed to the "support and dragline" effects.^[116] The $\text{PPDA-Nb}_2\text{CT}_x$ delivered an excellent capacity as 400 mAh g^{-1} under 0.1 A g^{-1} and the assembled $\text{PPDA-Nb}_2\text{CT}_x/\text{AC}$ LIC exhibited an energy density up to 100.3 Wh kg^{-1} under 53.6 W kg^{-1} .

4.1.5. Alloys

The alloy-based electrode materials have produced numerous concerns as the anode of metal-ion HCs by virtue of their

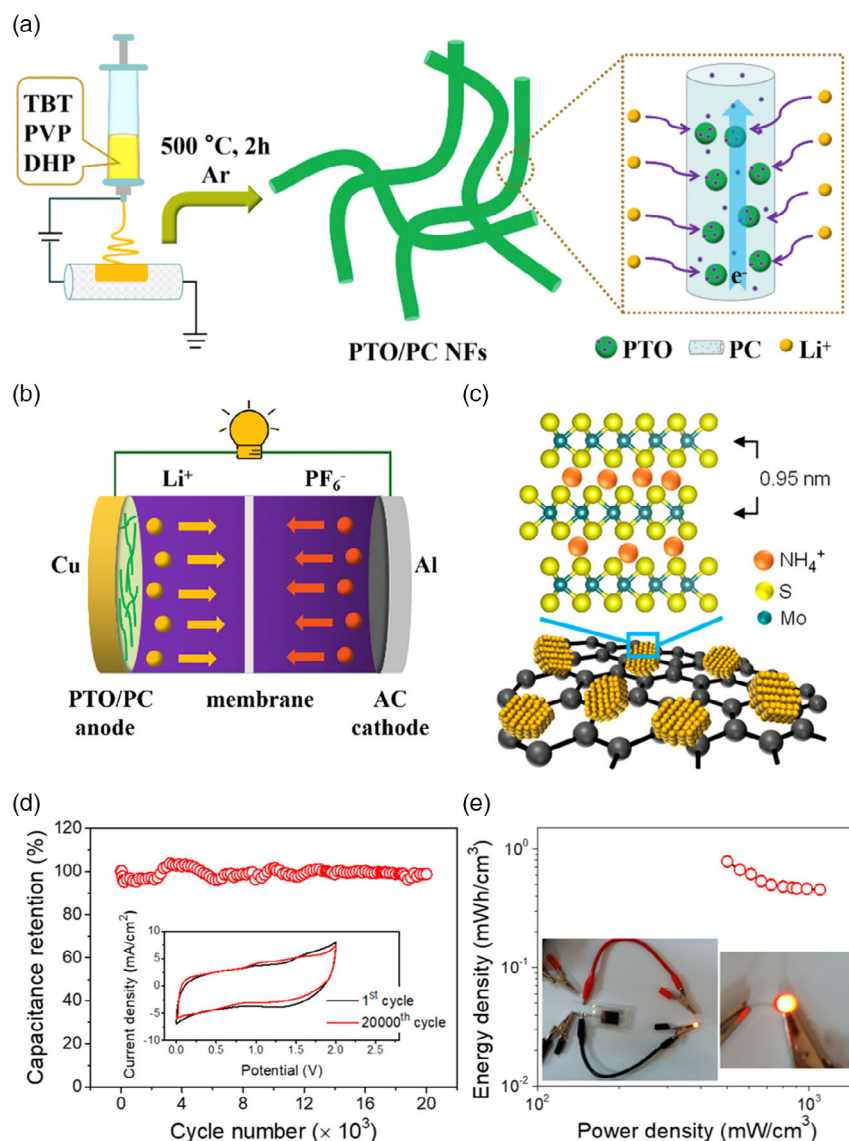


Figure 18. a) The schematic diagram of synthesizing TiO₂/P-doping carbon nanofibers (PTO/PC NFs) by electrospinning method. b) Schematic view about the fabrication of activated carbon (AC)//PTO/PC lithium-ion HCs (LICs). Reproduced with permission.^[109] Copyright 2020, Elsevier. c) Schematic diagram for NH₄⁺ intercalation into MoS₂ interlayer spacing. d) Cycling stability measurement of the MoS₂/rGO//Fe₂O₃/MnO₂ ASC during 20 000 cyclic voltammetry (CV) cycles under 100 mV s⁻¹, illustration was initial and final CV curves. e) Ragone plot for the MoS₂/rGO//Fe₂O₃/MnO₂ ASC, inset was digital photo about red LED driven by the ASC. Reproduced with permission.^[112] Copyright 2019, American Chemical Society.

remarkable theoretical capacity value and superior rate performance.^[117] Usually, the alloying reaction of metal ions and alloy anode materials conduct at low potential and help the metal-ion HCs have superior theoretical storage capacity and large operating voltage. For example, in LICs, the metal Si anode presented a theoretical Li-storage capacity as high as 3579 mAh g⁻¹ and the metal Sn anode performed a Li-storage theoretical capacity up to 994 mAh g⁻¹.^[118,119] Although the Sn, Sb, Si, and Bi alloy materials and their compounds have been widespread used in EES devices, the serious volume expansion and terrible cycle stability restrict their further development. Recently, the strategy of nanocrystallization, coating, and compositing with other materials is utilized to surmount the aforementioned shortcomings. For

example, Yuan and coworkers synthesized the 3D porous NaBi alloy by using electrochemical presodiation of bulk Bi.^[120] The constructed NaBi//AC NIC with porous NaBi anode and AC cathode exhibited an energy density up to 106.5 Wh kg⁻¹ under 105 W kg⁻¹ and good cycling stability of 98.6% reservation after 1000 cycles (Figure 19b–d).

4.1.6. MOFs

In recent years, MOFs, a novel porous crystalline material, are composed of inorganic and organic components linked by covalent coordination bonds, which have been a promising electrode material for the metal-ion HCs owing to their distinct merits,

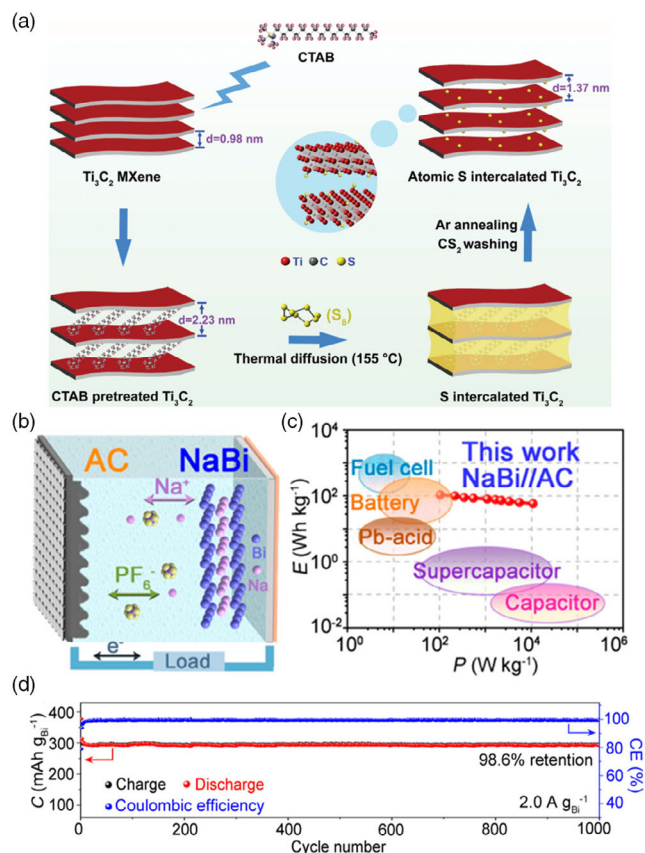


Figure 19. a) Schematic view about S atoms intercalated Ti₃C₂ preparation process. Reproduced with permission.^[115] Copyright 2019, Wiley-VCH. b) Schematic representation about the manufactured NaBi//AC sodium-ion HC (NIC). c) Ragone plots about the NaBi//AC NIC in comparison with other energy-storage systems. d) Cycling performance of NaBi//AC NIC at 2 A g⁻¹. Reproduced with permission.^[120] Copyright 2018, American Chemical Society.

including high specific surface area, abundant pores, and controllable morphology.^[7] The recent research about MOFs and MOFs-derived nanostructures has focused on regulating the chemical composition at the molecular level and exploiting highly porous framework, which is beneficial to increase the capacity and reduce ions transport pathways. For example, Dubal et al. prepared graphene-like nanosheets embedded with MnO₂ nanoparticles (MnO₂@C-NS) by exploiting a Mn-based MOF.^[121] When used as the anode material of LICs, it delivered a high reversible specific capacity of 1054 mAh g⁻¹ at 0.1 A g⁻¹ and good cycling stability with 90% retention over 1000 cycles. In addition, an LIC full cell was assembled with MnO₂@C-NS as anode and MOF-derived carbon nanosheets as cathode, and the specific energy achieved 166 Wh kg⁻¹ under 550 W kg⁻¹ and retained the 49.2 Wh kg⁻¹ at 3.5 kW kg⁻¹. In Wang's work, they engineered the porous polyhedral carbon (PC) and MoS₂-zeolitic imidazolate framework (ZIF) nanosheets by employing the ZIF-8 as precursors, which performed the capacitive and battery-like electrochemical behavior, respectively.^[122] Moreover, the MoS₂-ZIF/PC LIC was constructed with MoS₂-ZIF as positive

electrode, PC as negative electrode and Li-ion containing electrolyte, which behaved a high energy density of 155 Wh kg⁻¹ and a large power density of 20 kW kg⁻¹ as well as small capacity fade of 0.0021% per cycle over 10 000 cycles. The excellent performance can be attributed to the abundant pores and large surface area from MOFs, which effectively shortened the diffusion pathway and increased the active site, thus improving the capacity and rate capability.

4.2. Applications for Metal-Ion HCs

4.2.1. LICs

With the growing demand of electronic products and electric vehicles, the EES devices was required to provide high energy density and power density simultaneously. Currently, the commercial Li-ion batteries can achieve high energy density, but the low power density hindered its further development. Therefore, the novel LICs attracted widespread attention from scientific community, which was expected to possess the high energy density and power density. Different from Li-ion batteries, the LIC was composed of the capacitive cathode and battery anode, which will combine the high energy density of battery with the high-power density of supercapacitors.^[123] However, the sluggish kinetics of battery anode and kinetics mismatch between capacitive cathode and battery anode was key problem that need to be solved for LICs. For example, Chen et al. successfully anchored the MnO nanoparticles on the self-supported interconnected graphene scroll framework (MnO/GS), which provided a fast ion transport pathway and ameliorated the volume change, thus facilitating its kinetics and promoting the rate capability.^[124] The LIC was assembled with MnO/GS anode and AC cathode, which delivered a high energy density of 179.3 Wh kg⁻¹ under 139.2 W kg⁻¹ and 48.2 Wh kg⁻¹ under the high-power density of 11.7 kW kg⁻¹. Recently, Divya et al. designed the SnO₂@Graphite nanocomposites (SnO₂@G ncs) via the hydrothermal method coupled with the high-energy ball milling of SnO₂ and graphite.^[125] The assembled LICs with SnO₂@G ncs anode and AC cathode exhibited a high energy density of 172.33 Wh kg⁻¹ at 153 W kg⁻¹ and superior cycling performance with 90% retention after 9000 cycles. The study paved a way of incorporating alloy-type materials into intercalation-based anodes, which was favorable to improve the electrochemical performance.

4.2.2. NICs

In recent years, the NIBs had been proposed as a candidate for Li-ion battery owing to the low cost and rich resources of metal sodium than lithium. For the same reason, the NIC was also a good candidate for LICs, and the NIC was expected to obtain the high energy density and power density, which combined the advantages of NIBs and supercapacitors.^[126] Whereas, the sluggish kinetics of large-sized Na ion and kinetics imbalance from the battery anode and capacitive cathode was the critical issues affecting the electrochemical performance of NICs. Some recent reports had been used to address these problems. For example, Wang et al. engineered the 3D carbon framework (3DCF) with

interconnect and defective features through the electrolysis and calcination method, which was beneficial to promote the sodium-ion diffusion and storage.^[127] The NIC was fabricated with 3DCF as anode and sodium alginate-derived AC as cathode, which performed a high energy density of 133.2 Wh kg^{-1} and a high-power density of 20 kW kg^{-1} . In Huang's work, the electrochemically exfoliated graphite (EEG) was synthesized by the electrochemical method, which was confirmed to improve the reaction kinetics of Na-ion storage.^[128] the EEG anode and AC cathode were used to construct the NICs, which displayed an energy density of 90 Wh kg^{-1} and a high-power density of $17\,100 \text{ W kg}^{-1}$.

4.2.3. KICs

The LIC was earliest and most studied capacitors, but the expensive cost, scarcity, and uneven distribution of metal lithium inhibited its further development. By contrast, KIC was the promising candidate for LICs by virtue of its similar construction and reaction process with LICs and the low-cost and abundant resources of metal potassium.^[129] However, the electrochemical performance of KICs was hindered owing to the sluggish kinetics of large size K ion. Therefore, the current studies mainly focused on the electrode materials with large interlayer spacing, which was expected to promote K-ion transformation and improve the electrochemical performance. For example, Pham et al. prepared the multi-heteroatom-doped hard carbon (MHC) and AC foam (ACF) by utilizing the blue denim textile waste, respectively.^[130] Moreover, a dual-carbon KICs assembled with ACF cathode and MHC anode exhibited a high energy density of 181 Wh kg^{-1} at 70.4 W kg^{-1} and 61.8 Wh kg^{-1} at 4 kW kg^{-1} as well as 89% capacity retention over 5000 cycles. Then, they constructed the KICs by using recycled graphite (REG) from waste batteries as anode and AC as cathode, which achieved a high energy density of 84.5 Wh kg^{-1} at 400 W kg^{-1} .^[131] Thereafter, they further engineered the layered potassium niobate ($\text{K}_4\text{Nb}_6\text{O}_{17}$, KNO) nanosheet arrays and orange-peel-derived ACs (OPAC), which was used to the anode and cathode of KICs (KNO//OPAC KIC), respectively.^[132] The obtained KNO//OPAC KIC uncovered a high energy density of 116 Wh kg^{-1} and high-power density of $10\,808 \text{ W kg}^{-1}$ as well as the protruding cycling ability with 87% reservation after 5000 cycles. The superior performance was owing to the large interlayer distance of layered KNO, which was favorable to facilitate large-sized K-ion transportation.

4.2.4. ZICs

Currently, there have been numerous literatures on the monovalent metal-ion capacitors such as LICs, NICs, and KICs. However, these monovalent metal-ion capacitors faced serious safety issues, due to the active metal Li, Na, and K and the utilization of organic electrolytes. Meanwhile, the scarcity and uneven distribution of lithium sources resulted in the high cost and prohibited the further widely applications for LICs. In contrast, the zinc metal was very stable and low cost in the aqueous electrolyte, as well as the high theoretical capacity (823 mAh g^{-1}) and low redox potential (-0.76 V versus standard hydrogen electrode).^[133] Therefore, the ZICs have aroused extensive research

interest owing to its inherent advantages such as safety, high capacity, and energy density and fast charge-transfer dynamics. For example, in Wang's work, the ZICs was fabricated with Zn foil anode, AC cathode, and Zn-ion-containing electrolyte, in which AC was obtained from the biomass coconut shells.^[134] The as-assembled ZICs displayed a high energy density of 52.7 Wh kg^{-1} under 1725 W kg^{-1} and superior cycling stability with 91% retention over 20 000 cycles. Patil et al. engineered the graphene-boosted 2D-layered niobium oxyphosphide (rGO-NbPO) via a facile hydrothermal approach, which facilitated the fast diffusion of Zn ion and promoted the electrochemical performance.^[135] The ZICs was composed of Zn metal anode and rGO-NbPO cathode, which delivered an energy density of 56.03 Wh kg^{-1} and power density of 1000 W kg^{-1} . Since the ZICs was still in the infancy stage, some problems and challenges require further study and exploration, such as the sluggish diffusion of zinc ion, low utilization rate of zinc foil, and uncontrollable zinc dendrites.

4.2.5. DICs

Excitingly, the novel dual-ion batteries (DIBs) have motivated extensive research interests owing to their high operating voltage, inexpensiveness, and eco-friendliness.^[136,137] Taking the lithium-ion batteries (LIBs) as an example, the LIBs store energy through the "rocking-chair" mechanism and the lithium ions is repeatedly deintercalated/intercalated from the lithium-containing transition-metal oxide cathode and intercalate/deintercalated into the interlayer of the graphite anode through the electrolyte in the charge/discharge reaction.^[138] In contrast, the working mechanism of DIBs involve the storage of cations and anions from electrolyte separately in the anode and cathode during the charging/discharging reaction, which endow an enhanced capacity and eliminate the use of lithium-containing metals.^[139] Taking advantages of DIBs system, a special dual-ion capacitors (DICs) manufactured with a high potential supercapacitor-type cathode and a battery-type anode came to being based on a dual-ion-storage mechanism, which is expected to complete an increase about energy density, power density, and cycle performance at the same time.

At present, only a few articles about DICs have been appeared. For instance, Chen et al. prepared the nitrogen-abundant hierarchically porous carbon foams (NCF) using a carbonization-activation method (Figure 20a).^[140] The lithium-based DICs assembled from NCF had an energy density up to 179.5 Wh kg^{-1} under 150 W kg^{-1} (Figure 20b). Moreover, Feng et al. synthesized the carbon foam of microporous structure (CFMS) via the simple one-step carbonization and the symmetric potassium DICs was assembled with the CFMS as cathode and anode (Figure 20c).^[141] Such constructed potassium DICs exhibited an energy density as 58 Wh kg^{-1} under 1558.2 W kg^{-1} and ultra-long service life with 90% reservation over 10 000 cycles (Figure 20d,e). Meanwhile, the TEM, element mapping, and XRD were implemented to confirm the energy-storage mechanism of DICs.

Zhan et al. prepared the porous graphitic carbon (PGC) by a one-step activation/catalytic graphitization method.^[142] When the PGC used as the positive electrode material of DICs, it

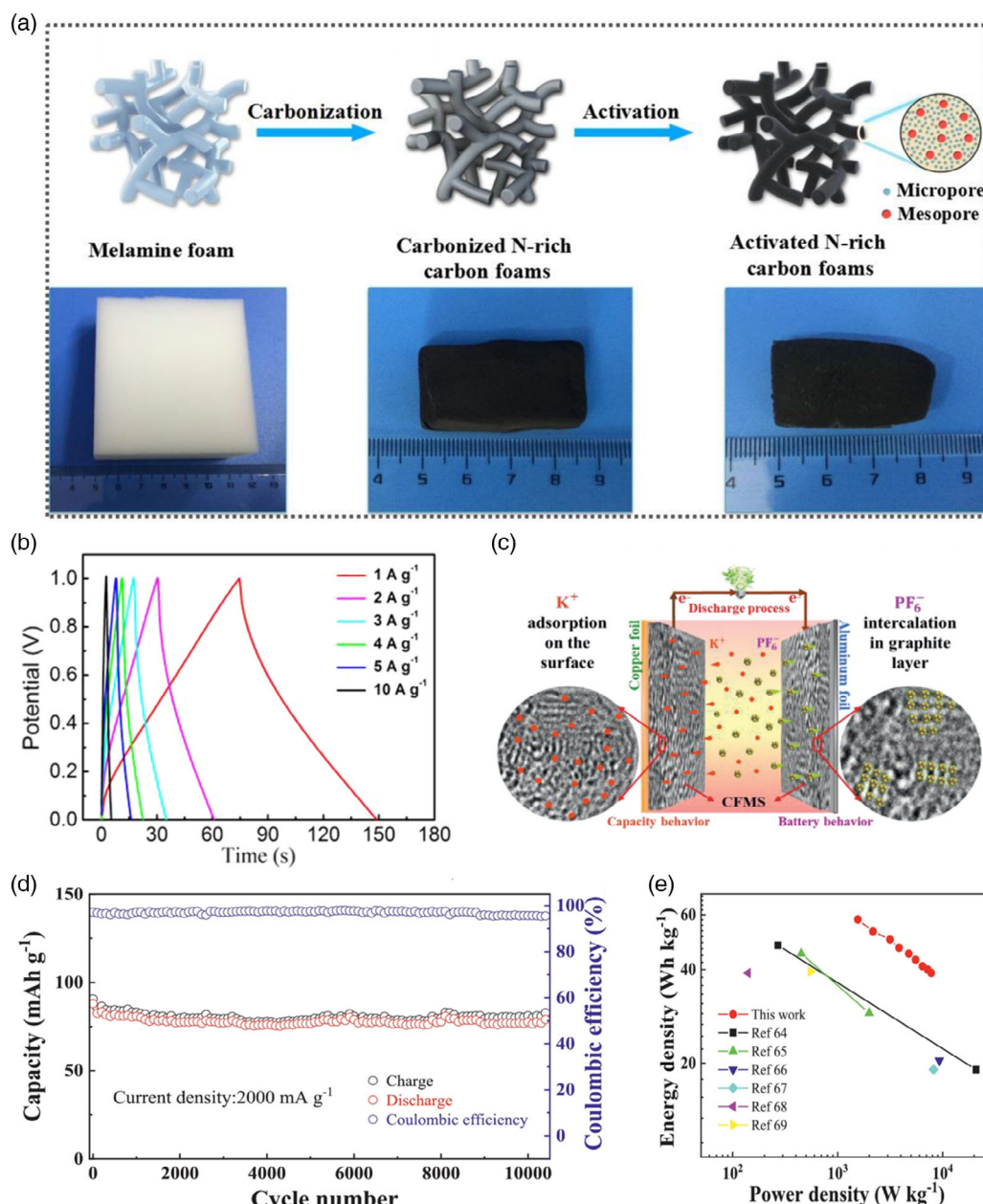


Figure 20. a) Schematic diagram of the manufacturing procedures about the 3D porous NCFs and relevant digital photos. b) Charge-discharge profiles under various current densities for the NCF-based symmetrical supercapacitors. Reproduced with permission.^[140] Copyright 2020, Elsevier BV. Electrochemical properties of carbon foam of microporous structure (CFMS)-based symmetric potassium dual-ion capacitors (PDICs). c) Schematic representation about symmetric PDICs in discharge stage. d) Cycling durability under 2000 mA g⁻¹. e) Ragone plots about PDICs compared with the previously reported values. Reproduced with permission.^[141] Copyright 2020, Elsevier BV.

exhibited LIC-like EDLC behavior in a wide range of low and medium potentials and showed DIB-like anion insertion/deintercalation behavior in a high potential range. In Chen's work, they successfully constructed sodium-based DICs by employing the N-doping microporous hard carbon as cathode and soft carbon as anode (Figure 21a), which performed a high energy density as 245.7 Wh kg⁻¹ under 1626 W kg⁻¹ with long cycle durability (1000 cycles).^[143] They conducted the ex situ element mapping and ex situ X-ray photoelectron spectroscopy

(XPS) under diverse charge/discharge stages to validate the operating mechanism of sodium-based DICs (Figure 21b-e). He et al. prepared the graphite@nano-silicon@carbon (Si/C) via interfacial adhesion between nanosilicon and graphite at the assistance of pitch.^[144] A dual-ion hybrid electrochemical device was fabricated with expanded graphite as anion-intercalation supercapacitor-type cathode and Si/C as cation intercalation battery-type anode, which showed high energy densities from 252 to 222.6 Wh kg⁻¹ under power densities from 215 to

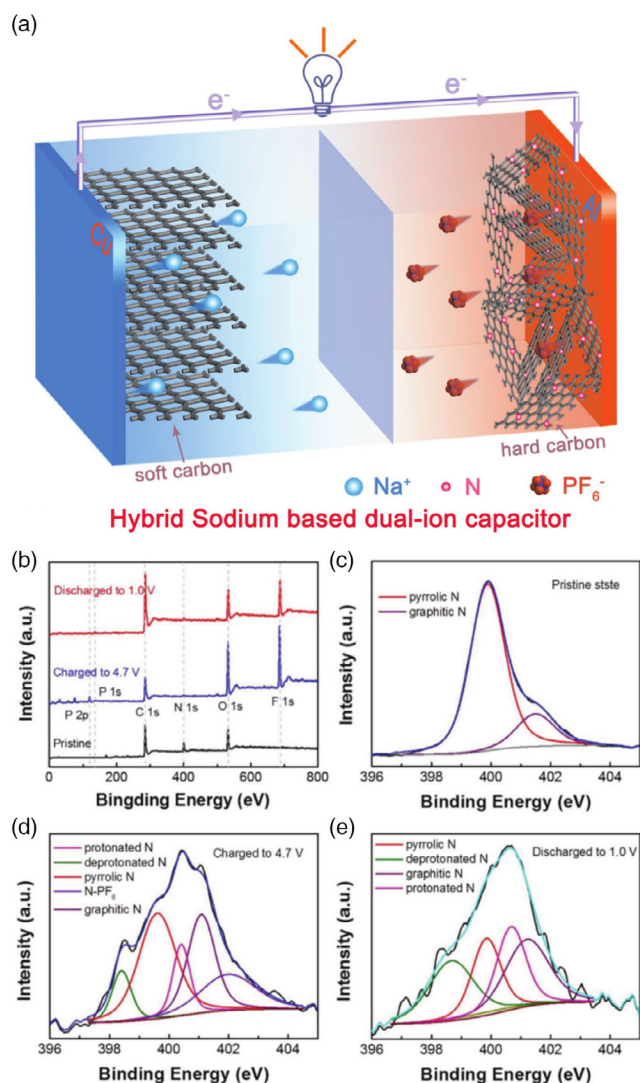


Figure 21. a) Schematic view about the charge and discharge process for sodium-based NICs. The XPS spectrum of the NICs electrodes under various charge/discharge states in half-cell. b) Full spectrum, high-resolution spectrum about N 1s in the stage for c) primitive, d) charge to 4.7 V, and e) discharge to 1.0 V. Reproduced with permission.^[143] Copyright 2018, Wiley-VCH.

5420 W kg⁻¹. Although the DICs exhibit outstanding advantages, its relevant study is still in its infancy. Therefore, the huge development potential for DICs remains to be developed and the in-depth research need to be conducted. Furthermore, the practical application potential for the current DICs required to be verified in prototypes of pouch cells and cylindrical cells, rather than in lab scales.

5. Summary and Outlook

With the increasing demand for electrical vehicles and electronic devices, the EES devices with high-power density as conventional capacitors, supercapacitors, and emerging capacitors has

achieved rapid development. In this minireview, we shortly summarize the development history about conventional capacitors, supercapacitors and emerging capacitors and the progress of related electrode materials, respectively. Although the electrochemical performance and application about capacitors, supercapacitors and emerging capacitors have been obviously improved and expanded, the following aspects remain to be further refined and improved: 1) With the rapidly development of clean and renewable energy, the research and report about EES devices have been sharply increased. However, the currently used concept and evaluated parameter is relatively confusion, which is not conducive to the long-term development of EES devices. For example, in supercapacitor, the term of battery-type electrode materials should be “specific capacity” (C g⁻¹ or mAh g⁻¹) instead of the “specific capacitance” (F g⁻¹) for pseudocapacitive materials. Therefore, the appraised indicators and criterion of EES devices should be normalized; 2) Although the electrode materials design has made great process, there is still a big gap between the displayed performance and theoretical value. Thus, the enormous efforts still need to focus on the improvement of synthesis techniques and the regulation of surface/interface, which is beneficial for the charge accumulation and effective electrolyte ions transport. Furthermore, to generate optimized electrode materials, the modification of electrode materials still need further exploration, including structure/morphology design, doping, compositing, and defect; 3) Regarding the basic charge-storage mechanism, the conflicting results are often reported, possibly because the research is on account of a finite number of electrochemical studies and ex situ characterization. Consequently, it is necessary to conduct collaborative research based on different in situ manipulation technologies to gain a thorough comprehending of the charge-storage mechanism for diverse electrode materials; 4) At present, most of the studies about EES devices only stay in the laboratory stage, and its practical application still needs to be taken into consideration. For example, some literatures about supercapacitors reported the excellent electrochemical performance, but its mass load of active materials was far smaller than 1 mg cm⁻². Such studies are meaningless and even misleading. The fabrication of pouch-cell-type EES devices with energy density at Ah level rather than laboratory level is important to step forward to the practical applications. Meanwhile, future research should also focus on the achievements of multifunctional EES devices having flexible, bendable, and transparent properties with sensing functions to the ambient environment. Therefore, the future research should be closer to reality and practical applications.

Acknowledgements

This work was financially supported by China Postdoctoral Science Foundation (Grant no. 2020M682560), The Science and Technology Innovation Program of Hunan Province (Grant no. 2020RC2024), Chinese Universities Scientific Fund (Grant no. 15052001), and Hunan Provincial Natural Science Foundation of China (Grant no. 2020JJ4175).

Conflict of Interest

The authors declare no conflict of interest.

Keywords

conventional capacitors, dual-ion capacitors, electrode materials, metal ion hybrid capacitors, supercapacitors

Received: November 28, 2021

Revised: February 21, 2022

Published online:

- [1] Z. Yang, J. Zhang, M. C. W. Kintner-Meyer, X. Lu, D. Choi, J. P. Lemmon, J. Liu, *Chem. Rev.* **2011**, 111, 3577.
- [2] Y. Shao, M. F. El-Kady, J. Sun, Y. Li, Q. Zhang, M. Zhu, H. Wang, B. Dunn, R. B. Kaner, *Chem. Rev.* **2018**, 118, 9233.
- [3] G. Z. Chen, *Int. Mater. Rev.* **2016**, 62, 173.
- [4] J. Yan, S. Li, B. Lan, Y. Wu, P. S. Lee, *Adv. Funct. Mater.* **2020**, 30, 1902564.
- [5] Q. Gou, S. Zhao, J. Wang, M. Li, J. Xue, *Nano-Micro Lett.* **2020**, 12, 98.
- [6] Z. Yao, Z. Song, H. Hao, Z. Yu, M. Cao, S. Zhang, M. T. Lanagan, H. Liu *Adv. Mater.* **2017**, 29, 1601727.
- [7] D.-G. Wang, Z. Liang, S. Gao, C. Qu, R. Zou, *Coord. Chem. Rev.* **2020**, 404, 213093.
- [8] Q. Guo, N. Chen, L. Qu, *Adv. Energy Sustainability Res.* **2021**, 2, 2100022.
- [9] X. Yu, S. Yun, J. S. Yeon, P. Bhattacharya, L. Wang, S. W. Lee, X. Hu, H. S. Park, *Adv. Energy Mater.* **2018**, 8, 1702930.
- [10] H. Luo, X. Zhou, C. Ellingford, Y. Zhang, S. Chen, K. Zhou, D. Zhang, C. R. Bowen, C. Wan, *Chem. Soc. Rev.* **2019**, 48, 4424.
- [11] H. Li, F. Liu, B. Fan, D. Ai, Z. Peng, Q. Wang, *Small Methods* **2018**, 2, 1700399.
- [12] B. Luo, X. Wang, E. Tian, H. Gong, Q. Zhao, Z. Shen, Y. Xu, X. Xiao, L. Li, *ACS Appl. Mater. Interfaces* **2016**, 8, 3340.
- [13] B. Luo, X. Wang, Q. Zhao, L. Li, *Compos. Sci. Technol.* **2015**, 112, 1.
- [14] G. Wang, Z. Lu, Y. Li, L. Li, H. Ji, A. Feteira, D. Zhou, D. Wang, S. Zhang, I. M. Reaney, *Chem. Rev.* **2021**, 121, 6124.
- [15] Z. Cai, X. Wang, B. Luo, W. Hong, L. Wu, L. Li, *J. Am. Ceram. Soc.* **2018**, 101, 1607.
- [16] L. Wu, X. Wang, Z. Shen, B. Luo, L. Li, *J. Am. Ceram. Soc.* **2017**, 100, 511.
- [17] Q. Zhao, H. Gong, X. Wang, B. Luo, L. Li, *Phys. Status Solidi A* **2016**, 213, 1077.
- [18] Y. Gogotsi, R. M. Penner, *ACS Nano* **2018**, 12, 2081.
- [19] R. Ma, Z. Chen, D. Zhao, X. Zhang, J. Zhuo, Y. Yin, X. Wang, G. Yang, F. Yi, *J. Mater. Chem. A* **2021**, 9, 11501.
- [20] M. A. Azam, N. S. N. Ramli, N. A. N. M. Nor, T. I. T. Nawi, *Int. J. Energy Res.* **2021**, 45, 8335.
- [21] M. Jayalakshmi, K. Balasubramanian, *Int. J. Electrochem. Sci.* **2008**, 3, 1196.
- [22] J. Ho, T. R. Jow, S. Boggs, *IEEE Electr. Insul. Mag.* **2010**, 26, 20.
- [23] J. Both, *IEEE Electr. Insul. Mag.* **2015**, 31, 24.
- [24] A. Noori, M. F. El-Kady, M. S. Rahmanifar, R. B. Kaner, M. F. Mousavi, *Chem. Soc. Rev.* **2019**, 48, 1272.
- [25] A. Nishino, *J. Power Sources* **1996**, 60, 137.
- [26] G. Z. Chen, *Prog. Nat. Sci.* **2013**, 23, 245.
- [27] C. Liu, Z. G. Neale, G. Cao, *Mater Today* **2016**, 19, 109.
- [28] C. Hou, W. Huang, W. Zhao, D. Zhang, Y. Yin, X. Li, *ACS Appl. Mater. Interfaces* **2017**, 9, 20484.
- [29] Qi. Li, L. Chen, M. R. Gadinski, S. Zhang, G. Zhang, H. U. Li, E. Iagodkine, A. Haque, L.-Q. Chen, T. N. Jackson, Q. Wang, *Nature* **2015**, 523, 576.
- [30] B. Chu, X. Zhou, K. Ren, B. Neese, M. Lin, Q. Wang, F. Bauer, Q. M. Zhang, *Science* **2006**, 313, 334.
- [31] B. Luo, X. Wang, H. Wang, Z. Cai, L. Li, *Compos. Sci. Technol.* **2017**, 151, 94.
- [32] B. Luo, X. Wang, Y. Wang, L. Li, *J. Mater. Chem. A* **2014**, 2, 510.
- [33] B. Luo, X. Wang, H. Sun, L. Li, *Appl. Phys. Lett.* **2016**, 108, 243901.
- [34] T. D. Huan, S. Boggs, G. Teyssedre, C. Laurent, M. Cakmak, S. Kumar, R. Ramprasad, *Prog. Mater. Sci.* **2016**, 83, 236.
- [35] B. Luo, X. Wang, E. Tian, H. Qu, Q. Zhao, Z. Cai, H. Wang, W. Feng, B. Li, L. Li, *J. Am. Ceram. Soc.* **2018**, 101, 2976.
- [36] B. Luo, X. Wang, E. Tian, H. Song, Q. Zhao, Z. Cai, W. Feng, L. Li, *J. Eur. Ceram. Soc.* **2018**, 38, 1562.
- [37] H. Zhang, T. Wei, Q. Zhang, W. Ma, P. Fan, D. Salamon, S.-T. Zhang, B. Nan, H. Tan, Z.-G. Ye, *J. Mater. Chem. C* **2020**, 8, 16648.
- [38] B. Luo, X. Wang, E. Tian, H. Song, H. Wang, L. Li, *ACS Appl. Mater. Interfaces* **2017**, 9, 19963.
- [39] C. Zhu, Z. Cai, B. Luo, L. Guo, L. Li, X. Wang, *J. Mater. Chem. A* **2020**, 8, 683.
- [40] H. Zhang, M. A. Marwat, B. Xie, M. Ashtar, K. Liu, Y. Zhu, L. Zhang, P. Fan, C. Samart, Z.-G. Ye, *ACS Appl. Mater. Interfaces* **2020**, 12, 1.
- [41] D. Q. Tan, *Adv. Funct. Mater.* **2020**, 30, 1808567.
- [42] L. Liu, J. Qu, A. Gu, B. Wang, *J. Mater. Chem. A* **2020**, 8, 18515.
- [43] G. Zhang, Q. Li, E. Allahyarov, Y. Li, L. Zhu, *ACS Appl. Mater. Interfaces* **2020**, 13, 37939.
- [44] B. Fan, M. Zhou, C. Zhang, D. He, J. Bai, *Prog. Polym. Sci.* **2019**, 97, 101143.
- [45] B. Luo, Z. Shen, Z. Cai, E. Tian, Y. Yao, B. Li, A. Kursumovic, J. L. Macmanus-Driscoll, L. Li, L.-Q. Chen, X. Wang, *Adv. Funct. Mater.* **2021**, 31, 2007994.
- [46] H. Palneedi, M. Peddigari, G.-T. Hwang, D.-Y. Jeong, J. Ryu, *Adv. Funct. Mater.* **2018**, 28, 1803665.
- [47] K. Hong, T. H. Lee, J. M. Suh, S.-H. Yoon, H. W. Jang, *J. Mater. Chem. C* **2019**, 7, 9782.
- [48] M. Feng, Y. Feng, T. Zhang, J. Li, Q. Chen, Q. Chi, Q. Lei, *Adv. Sci.* **2021**, 8, 2102221.
- [49] Y.-X. Liu, S.-F. Wang, Y.-F. Hsu, W.-Y. Yeh, *Surf. Coat. Technol.* **2018**, 344, 507.
- [50] P. Zhao, Z. Cai, L. Chen, L. Wu, Y. Huan, L. Guo, L. Li, H. Wang, X. Wang, *Energy Environ. Sci.* **2020**, 13, 4882.
- [51] H. Pan, S. Lan, S. Xu, Q. Zhang, H. Yao, Y. Liu, F. Meng, E.-J. Guo, L. Gu, D. Yi, X. Renshaw Wang, H. Huang, J. L. MacManus-Driscoll, L.-Q. Chen, K.-J. Jin, C.-W. Nan, Y.-H. Lin, *Science* **2021**, 374, 100.
- [52] H. Helmholtz, *Ann. Phys.* **1853**, 165, 211.
- [53] H. I. Becker, *Low voltage electrolytic capacitor*, United States patent US2800616A **1957**.
- [54] A. Burke, *J. Power Sources* **2000**, 91, 37.
- [55] J. R. Miller, *Market and Applications of Electrochemical Capacitors*, Wiley-VCH Verlag GmbH & Co. KGaA **2013**, pp 509–526.
- [56] P. Simon, Y. Gogotsi, B. Dunn, *Science* **2014**, 343, 1210.
- [57] L. L. Zhang, X. S. Zhao, *Chem. Soc. Rev.* **2009**, 38, 2520.
- [58] V. Augustyn, P. Simon, B. Dunn, *Energy Environ. Sci.* **2014**, 7, 1597.
- [59] V. Sudha, M. V. Sangaranarayanan, *J. Phys. Chem. B* **2002**, 106, 2699.
- [60] R.-R. Bi, X.-L. Wu, F.-F. Cao, L.-Y. Jiang, Y.-G. Guo, L.-J. Wan, *J. Phys. Chem. C* **2010**, 114, 2448.
- [61] L. Kong, C. Zhang, S. Zhang, J. Wang, R. Cai, C. Lv, W. Qiao, L. Ling, D. Long, *J. Mater. Chem. A* **2014**, 2, 17962.
- [62] Jintao. Zhang, X. S. Zhao, *ChemSusChem* **2012**, 5, 818.
- [63] L. Wen, F. Li, H.-M. Cheng, *Adv. Mater.* **2016**, 28, 4306.
- [64] Q. Wang, J. Yan, Z. Fan, *Energy Environ. Sci.* **2016**, 9, 729.
- [65] P. Simon, Y. Gogotsi, *Nat. Mater.* **2008**, 7, 845.
- [66] F. Wei, X. He, L. Ma, H. Zhang, N. Xiao, J. Qiu, *Nano-Micro Lett.* **2020**, 12, 82.
- [67] L. Wang, X. Li, R. Liu, Y. Wang, Y. Bai, Y. Liu, Y. Ma, G. Yuan, Z. Guo, *Nano Energy* **2021**, 80, 105572.

- [68] H. Zhang, J. Xue, S. Wang, Y. Song, J. Zhao, Y. Li, *J. Energy Storage* **2022**, 47, 103657.
- [69] Z. Liu, A. Qin, K. Zhang, P. Lian, X. Yin, H. Tan, *Nano Energy* **2021**, 90, 106540.
- [70] H. Li, Y. Gong, C. Fu, H. Zhou, W. Yang, M. Guo, M. Li, Y. Kuang, *J. Mater. Chem. A* **2017**, 5, 3875.
- [71] Y. Sim, S. Surendran, H. Cha, H. Choi, M. Je, S. Yoo, D. Chan Seok, Y. Ho Jung, C. Jeon, D. Jin Kim, M.-K. Han, H. Choi, U. Sim, J. Moon, *Chem. Eng. J.* **2022**, 428, 132086.
- [72] Z. Li, S. Gadipelli, H. Li, C. A. Howard, D. J. L. Brett, P. R. Shearing, Z. Guo, I. P. Parkin, F. Li, *Nat. Energy* **2020**, 5, 160.
- [73] Y. Shi, L. Peng, Y. Ding, Y. Zhao, G. Yu, *Chem. Soc. Rev.* **2015**, 44, 6684.
- [74] L. Pan, G. Yu, D. Zhai, H. R. Lee, W. Zhao, N. Liu, H. Wang, B. C.-K. Tee, Y. Shi, Y. Cui, Z. Bao, *Proc. Natl. Acad. Sci. U.S.A.* **2012**, 109, 9287.
- [75] J. Huang, K. Wang, Z. Wei, *J. Mater. Chem.* **2010**, 20, 1117.
- [76] B. Wang, J. Zhao, D. Zhang, H. Zhang, K. Cheng, K. Ye, K. Zhu, J. Yan, D. Cao, W. Jiao, Y. Liu, G. Wang, *Appl. Surf. Sci.* **2019**, 474, 147.
- [77] H. Wang, H. Yang, Y. Diao, Y. Lu, K. Chrulski, J. M. D'Arcy, *ACS Nano* **2021**, 15, 7799.
- [78] A. Kumar Das, B. Ramulu, E. Girija Shankar, J. Su Yu, *Chem. Eng. J.* **2022**, 429, 132486.
- [79] X. Chang, M. F. El-Kady, A. Huang, C.-W. Lin, S. Aguilar, M. Anderson, J. Z. J. Zhu, R. B. Kaner, *Adv. Funct. Mater.* **2021**, 31, 2102397.
- [80] X. Wang, Y. Wang, D. Liu, X. Li, H. Xiao, Y. Ma, M. Xu, G. Yuan, G. Chen, *ACS Appl. Mater. Interfaces* **2021**, 13, 30633.
- [81] T. Brousse, D. Bélanger, J. W. Long, *J. Electrochem. Soc.* **2015**, 162, A5185.
- [82] D. Majumdar, T. Maiyalagan, Z. Jiang, *Chemelectrochem* **2019**, 6, 4343.
- [83] W. Zuo, R. Li, C. Zhou, Y. Li, J. Xia, J. Liu, *Adv. Sci.* **2017**, 4, 1600539.
- [84] T. Wang, H. C. Chen, F. Yu, X. S. Zhao, H. Wang, *Energy Storage Mater.* **2019**, 16, 545.
- [85] S. Chandra Sekhar, G. Nagaraju, J. S. Yu, *Nano Energy* **2018**, 48, 81.
- [86] Z. Wu, Y. Zhu, X. Ji, *J. Mater. Chem. A* **2014**, 2, 14759.
- [87] Y. Xu, Z. Liu, D. Chen, Y. Song, R. Wang, *Prog. Nat. Sci.* **2017**, 27, 197.
- [88] J. Sun, X. Du, R. Wu, Y. Zhang, C. Xu, H. Chen, *ACS. Appl. Energy Mater.* **2020**, 3, 8026.
- [89] V. D. Nithya, N. S. Arul, *J. Power Sources* **2016**, 327, 297.
- [90] S. B. Bandgar, M. M. Vadiyar, Y.-C. Ling, J.-Y. Chang, S.-H. Han, A. V. Ghule, S. S. Kolekar, *ACS Appl. Energy Mater.* **2018**, 1, 638.
- [91] F. Saleki, A. Mohammadi, S. E. Moosavifard, A. Hafizi, M. R. Rahimpour, *J. Colloid Interfaces Sci.* **2019**, 556, 83.
- [92] L. Liao, H. Zhang, W. Li, X. Huang, Z. Xiao, K. Xu, J. Yang, R. Zou, J. Hu, *J. Alloy Compd.* **2017**, 695, 3503.
- [93] H. Mei, Z. Huang, B. Xu, Z. Xiao, Y. Mei, H. Zhang, S. Zhang, D. Li, W. Kang, D. F. Sun, *Nano-Micro Lett.* **2020**, 12, 61.
- [94] H. Tong, S. Yue, F. Jin, L. Lu, Q. Meng, X. Zhang, *Ceram. Int.* **2018**, 44, 3113.
- [95] A. M. Patil, N. Kitiphatpiboon, X. An, X. Hao, S. Li, X. Hao, A. Abudula, G. Guan, *ACS Appl. Mater. Interfaces* **2020**, 12, 52749.
- [96] S. Liu, L. Kang, J. Hu, E. Jung, J. Zhang, S. C. Jun, Y. Yamauchi, *ACS Energy Lett.* **2021**, 6, 3011.
- [97] W. Yang, J. Yang, J. J. Byun, F. P. Moissinac, J. Xu, S. J. Haigh, M. Domingos, M. A. Bissett, R. A. W. Dryfe, S. Barg, *Adv. Mater.* **2019**, 31, 1902725.
- [98] W. Yang, J. J. Byun, J. Yang, F. P. Moissinac, Y. Peng, G. Tontini, R. A. W. Dryfe, S. Barg, *Energy Environ. Mater.* **2020**, 3, 380.
- [99] L. Dong, W. Yang, W. Yang, Y. Li, W. Wu, G. Wang, *J. Mater. Chem. A* **2019**, 7, 13810.
- [100] C. Han, X. Wang, J. Peng, Q. Xia, S. Chou, G. Cheng, Z. Huang, W. Li, *Polymers* **2021**, 13, 2137.
- [101] G. G. Amatucci, F. Badway, A. Du Pasquier, T. Zheng, *J. Electrochem. Soc.* **2001**, 148, A930.
- [102] Z. Chen, V. Augustyn, X. Jia, Q. Xiao, B. Dunn, Y. Lu, *ACS Nano* **2012**, 6, 4319.
- [103] A. Le Comte, Y. Reynier, C. Vincens, C. Leys P. Azaïs, *J. Power Sources* **2017**, 363, 34.
- [104] Y. Tian, R. Amal, D.-W. Wang, *Front. Energy Res.* **2016**, 4, 34.
- [105] C. Zhang, Y. Xu, G. Du, Y. Wu, Y. Li, H. Zhao, U. Kaiser, Y. Lei, *Nano Energy* **2020**, 72, 104661.
- [106] L.-F. Que, F.-D. Yu, Z.-B. Wang, D.-M. Gu, *Small* **2018**, 14, 1704508.
- [107] Y. Luan, R. Hu, Y. Fang, K. Zhu, K. Cheng, J. Yan, K. Ye, G. Wang, D. Cao, *Nano-Micro Lett.* **2019**, 11, 30.
- [108] X. Liu, Y. Sun, Y. Tong, X. Wang, J. Zheng, Y. Wu, H. Li, L. Niu, *Nano Energy* **2021**, 86, 106070.
- [109] J. Huo, Y. Xue, X. Wang, Y. Liu, L. Zhang, S. Guo, *J. Power Sources* **2020**, 473, 228551.
- [110] H. Liang, Y. Zhang, S. Hao, L. Cao, Y. Li, Q. Li, D. Chen, X. Wang, X. Guo, H. Li, *Energy Storage Mater.* **2021**, 40, 250.
- [111] Z. Hu, Q. Liu, S.-L. Chou, S.-X. Dou, *Adv. Mater.* **2017**, 29, 1700606.
- [112] D. Sarkar, D. Das, S. Das, A. Kumar, S. Patil, K. K. Nanda, D. D. Sarma, A. Shukla, *ACS Energy Lett.* **2019**, 4, 1602.
- [113] J. Ge, B. Wang, J. Wang, Q. Zhang, B. Lu, *Adv. Energy Mater.* **2020**, 10, 1903277.
- [114] X. Wang, S. Kajiyama, H. Iinuma, E. Hosono, S. Oro, I. Moriguchi, M. Okubo, A. Yamada, *Nat. Commun.* **2015**, 6, 6544.
- [115] J. Luo, J. Zheng, J. Nai, C. Jin, H. Yuan, O. Sheng, Y. Liu, R. Fang, W. Zhang, H. Huang, Y. Gan, Y. Xia, C. Liang, J. Zhang, W. Li, X. Tao, *Adv. Funct. Mater.* **2019**, 29, 1808107.
- [116] M.-C. Liu, B.-M. Zhang, Y.-S. Zhang, D.-T. Zhang, C.-Y. Tian, L.-B. Kong, Y.-X. Hu, *Batteries Supercaps* **2021**, 4, 1473.
- [117] M. Arnaiz, J. L. Gómez-Cámer, J. Ajuria, F. Bonilla, B. Acebedo, M. Jáuregui, E. Goikolea, M. Galceran, T. Rojo, *Chem. Mater.* **2018**, 30, 8155.
- [118] H. Jiang, S. Wang, D. Shi, F. Chen, Y. Shao, Y. Wu, X. Hao, *J. Mater. Chem. A* **2021**, 9, 1134.
- [119] F. Sun, J. Gao, Y. Zhu, X. Pi, L. Wang, X. Liu, Y. Qin, *Sci. Rep.* **2017**, 7, 40990.
- [120] Y. Yuan, C. Wang, K. Lei, H. Li, F. Li, J. Chen, *ACS Cent. Sci.* **2018**, 4, 1261.
- [121] D. P. Dubal, K. Jayaramulu, J. Sunil, Š. Kment, P. Gomez-Romero, C. Narayana, R. Zbořil, R. A. Fischer, *Adv. Funct. Mater.* **2019**, 29, 1900532.
- [122] R. Wang, D. Jin, Y. Zhang, S. Wang, J. Lang, X. Yan, L. Zhang, *J. Mater. Chem. A* **2017**, 5, 292.
- [123] B. Li, J. Zheng, H. Zhang, L. Jin, D. Yang, H. Lv, C. Shen, A. Shellikeri, Y. Zheng, R. Gong, J. P. Zheng, C. Zhang, *Adv. Mater.* **2018**, 30, 1705670.
- [124] P. Chen, W. Zhou, Z. Xiao, S. Li, H. Chen, Y. Wang, Z. Wang, W. Xi, X. Xia, S. Xie, *Energy Storage Mater.* **2020**, 33, 298.
- [125] D. Ml, S. Praneetha, Y.-S. Lee, V. Aravindan, *Composites, Part B* **2021**, 230, 109487.
- [126] Z. Zhang, Z. Gu, C. Zhang, J. Li, C. Wang, *Batteries Supercaps* **2021**, 4, 1680.
- [127] P. Wang, Y. Bingjun, G. Zhang, L. Zhang, H. Jiao, J. Chen, X. Yan, *Chem. Eng. J.* **2018**, 353, 453.
- [128] T. Huang, Z. Liu, F. Yu, F. Wang, D. Li, L. Fu, Y. Chen, H. Wang, Q. Xie, S. Yao, Y. Wu, *ACS Appl. Mater. Interfaces* **2020**, 12, 52635.
- [129] M. Liu, L. Chang, Z. Le, J. Jiang, J. Li, H. Wang, C. Zhao, T. Xu, P. Nie, L. Wang, *ChemSusChem* **2020**, 13, 5837.
- [130] H. D. Pham, J. F. S. Fernando, M. Horn, J. MacLeod, N. Motta, W. O. S. Doherty, A. Payne, A. K. Nanjundan, D. Golberg, D. Dubal, *Electrochim. Acta* **2021**, 389, 138717.

- [131] H. Duc Pham, C. Padwal, J. F. S. Fernando, T. Wang, T. Kim, D. Golberg, D. P. Dubal, *Batteries Supercaps* **2022**, 5, e202100335.
- [132] H. D. Pham, N. R. Chodankar, S. D. Jadhav, K. Jayaramulu, A. K. Nanjundan, D. P. Dubal, *Energy Storage Mater.* **2021**, 34, 475.
- [133] J. Yin, W. Zhang, N. A. Alhebshi, N. Salah, H. N. Alshareef, *Adv. Energy Mater.* **2021**, 11, 2100201.
- [134] H. Wang, M. Wang, Y. Tang, *Energy Storage Mater.* **2018**, 13, 1.
- [135] S. Patil, N. Chodankar, H. Seung Kyu, G. S. R. Raju, K. S. Ranjith, Y. S. Huh, Y. K. Han, *Energy Storage Mater.* **2022**, 45, 1040.
- [136] H. Jiang, Z. Wei, L. Ma, Y. Yuan, J. J. Hong, X. Wu, D. P. Leonard, J. Holoubek, J. J. Razink, W. F. Stickle, F. Du, T. Wu, J. Lu, X. Ji, *Angew. Chem., Int. Ed.* **2019**, 58, 5286.
- [137] L. Zhang, H. Wang, X. Zhang, Y. Tang, *Adv. Funct. Mater.* **2021**, 31, 2010958.
- [138] H. Xia, Y. Tang, O. I. Malyi, Z. Zhu, Y. Zhang, W. Zhang, X. Ge, Y. Zeng, X. Chen, *Adv. Mater.* **2021**, 33, 2004998.
- [139] S. Rothermel, P. Meister, G. Schmuelling, O. Fromm, H.-W. Meyer, S. Nowak, M. Winter, T. Placke, *Energ. Environ. Sci.* **2014**, 7, 3412.
- [140] Y. Chen, X. Qiu, L.-Z. Fan, *J. Energy Chem.* **2020**, 48, 187.
- [141] Y. Feng, S. Chen, J. Wang, B. Lu, *J. Energy Chem.* **2020**, 43, 129.
- [142] C. Zhan, X. Zeng, X. Ren, Y. Shen, R. Lv, F. Kang, Z.-H. Huang, *J. Energy Chem.* **2020**, 42, 180.
- [143] S. Chen, J. Wang, L. Fan, R. Ma, E. Zhang, Q. Liu, B. Lu, *Adv. Energy Mater.* **2018**, 8, 1800140.
- [144] S. He, S. Wang, H. Chen, X. Hou, Z. Shao, *J. Mater. Chem. A* **2020**, 8, 2571.



Jiale Sun is now a Ph.D. student in the College of Chemistry and Chemical Engineering at Hunan University. He received his master of engineering degree from the North University of China in 2021. His current research interests are the preparation of electrode materials and their applications in supercapacitors and electrochemical CO₂ reduction reactions.



Bingcheng Luo is a professor in the College of Science at China Agricultural University. He received his B.S. from the China University of Geosciences, Beijing, and Ph.D. from Tsinghua University, and completed postdoctoral research training at the University of Cambridge. His research interests are in the experimental development and multiscale modeling of advanced functional materials, including ferroelectric ceramics, layered composites, and inorganic/organic composites, and applications in electronics, energy storage, and agriculture.



Huanxin Li is currently working in the Department of Engineering at the University of Cambridge as a research associate. He leads multiple tasks including supercapacitors, Li-ion batteries, Li-S batteries, metal-air batteries, and wearable devices as a project team leader for the energy-storage lab. Dr. Li carried out his doctoral training at the Department of Chemistry and Chemical Engineering, Hunan University from 2014 to 2019, and the Department of Chemistry at King's College London, UK, as a visiting Ph.D. candidate during 2019. Dr. Li gained multidisciplinary research interests and experiences in materials science, electrocatalysts, batteries, and thermal cells.